7-2015

A study of the selective laser alloying of elemental titanium and boron powder

Yingbin Hu
University of Texas-Pan American

A STUDY OF THE SELECTIVE LASER ALLOYING OF ELEMENTAL TITANIUM AND BORON POWDER

A Thesis

by

YINGBIN HU

Submitted to the Graduate School of
The University of Texas-Pan American
In partial fulfillment of the requirements for the degree of

MASTER OF SCIENCE

July 2015

Major Subject: Manufacturing Engineering

A STUDY OF THE SELECTIVE LASER ALLOYING OF ELEMENTAL TITANIUM AND BORON POWDER

A Thesis
by
YINGBIN HU

COMMITTEE MEMBERS

Dr. Jianzhi Li
Chair of Committee

Dr. Miguel A. Gonzalez
Committee Member

Dr. Douglas Timmer
Committee Member

Dr. Robert Jones
Committee Member

July 2015

ABSTRACT

Hu, Yingbin, A Study of the Selective Laser Alloying of Elemental Titanium and Boron Powder. Master of Science (MS), July, 2015, 63 pp, 5 tables, 20 figures, 45 titles.

To better understand the selective laser alloying process of elemental titanium and boron powder, theoretic models are created which takes material related, reaction related, laser related, and other affecting factors into consideration. These models do help interpret the corresponding experiment results. In turn, the related experiment results validate the theoretic models created. In practice, the experiments with two different molar ratios of 1:2 and 4:1 between titanium and boron are carried out. The huge amount of energy released because of reaction between titanium and boron during laser irradiation makes it hard to understand and control the alloying process. At the same time, the energy released can also be utilized to lower the laser power and speed up the scanning speed. In the end, laser parameters are optimized to build solid parts with good quality of top surface finish and only few defects inside.

DEDICATION

I dedicate my thesis work to my family that has always been there for me, even though they live far away in China. A special feeling of gratitude to my loving parents, their support and encouragement push me forward.

此文献予我的家庭，虽然远隔万里，你们却一直相伴左右。对父母的敬爱之情难以言表，是你们的支持与鼓励使我前行。

ACKNOWLEDGMENTS

First and foremost, I offer my sincerest gratitude to my supervisor, Dr. Jianzhi Li for his countless hours of coaching, encouragement, and most of all his patience throughout my whole master program. His guidance helped me in all the time of research and writing of this thesis. My appreciation also goes to Dr. Miguel A. Gonzalez, Dr. Douglas Timmer and Dr. Robert Jones who gave me a lot of constructive suggestions and agreed to serve on my committee.

I would like to show my appreciation to Hugo Montiel for helping me develop my technology skills, e.g. milling machine and XRD, to Cynthia Barros for helping me to manage time, to Juan Carlos for the many hours of helping of my projects, to Dr. Anfu Guo for helping me with the arrangement of my thesis.

My additional thanks go to the engineering department for allowing me to conduct my research and providing any assistance requested.

TABLE OF CONTENTS

LIST OF TABLES

Page

LIST OF FIGURES

CHAPTER I

INTRODUCTION

1.1 Overview of this Chapter

This chapter introduces the topic that will be studied for the following chapters. Section 1.2 explains the reason why this topic is put forward. And Section 1.3 lists the objectives that need achieving by this thesis. The affecting factors and problem faced are discussed in Section 1.4. Section 1.5 is a brief organization of the whole thesis.

1.2 Selective Laser Alloying of the Mixture of Titanium and Boron Powder

Due to their high tensile strength to density ratio, excellent corrosion resistance and good biocompatibility, titanium and its alloys are widely used in astronautic, biomedical and auto industries (Kartal, Timur, Urgen, and Erdemir, 2010). Among all its alloys, the boride titanium (TiBw) which exhibits excellent corrosion resistance, hardness and electrical conductivity (Schmidt, Boehling, Burkhardt, and Grin, 2007) is the focus of this thesis. Table 1.1 shows the comparison of properties between Ti, TiB, and TiB_2 (Atri et al., 1999, Panda et al., 2003, Ravi Chandran et al., 2004).

Ti-B alloys can be synthesized via conventional cast metallurgy approach and powder metallurgy technique. For surface hardening of titanium, laser-aided methods gain its popularity among researchers. However, since titanium and boron can react with each other which makes

the process hard to control, selective laser melting (SLM) method is seldom used to process the mixture of titanium and boron powder. Due to the reason that SLM is an energy-demanding process, the understanding of the reactive powder system can be utilized to assist in the SLM process by saving laser energy input and time.

Table 1.1 – Properties of Ti, TiB, and TiB_2

Property	Ti	TiB	TiB_2
Density (g/cm^3)	4.57	4.56	4.52
Elastic modulus (GPa)	110	371	540
Coeff. of thermal exp. At RT (^oC)	8.6×10^{-6}	7.15×10^{-6}	6.2×10^{-6}
Vickers hardness (kg/mm^2)	150	1,800	2,200
Melting/decomposition temp. (^oC)	1,668	2,200	2,970

1.3 Objectives of the Present Research

As mentioned above, the focus of this thesis is to understand the selective laser alloying process of the mixture of titanium and boron powder. To have a better understanding of the process, theoretic models are developed to interpret corresponding experiment results. In turn, the experiment results can also test the accuracy of the models created. The main objectives of this thesis are as follows:

- To investigate and understand the selective laser alloying process of the mixture of titanium and boron powder.
- To develop theoretic models which can contribute to interpreting the selective laser alloying process phenomena.
- To test and verify the developed models by the corresponding experiment results.

- To build solid parts (multiple layers) with the parameters optimized by taking advantage of the reaction between titanium and boron.

1.4 Affecting Factors

Figure 1.1 shows the schematic overview of SLM process. First, a 3D CAD file created by 3D modeling software with standard STL (solid to layer) format is sliced to create a 2-dimensional (2D) profile for each layer. This sliced file prepared by the specific software can also define supports, processing parameters to the corresponding machine. When the file is uploaded and selected, the machine starts working under a controlled low-oxygen atmosphere. As is shown in Figure 1.1, the dosing metallic powder from the hopper will be distributed evenly by the recoater. Then, laser beam fuses the selected area of this layer based on the sliced 3D file. After the fusing of this layer, the elevator will drive the whole platform one layer down (Z direction) which gives space for the recoater to distribute another layer of powder. Layer after layer, the final object is created. The laser irradiation process is carried out under an inert atmosphere to avoid oxidation of the powder. Once complete, the object will be removed by chopping down the support underneath and the powder left can be recycled after sieving. The scanning mirrors shown in Figure 1.1 can direct the laser beam in X and Y directions.

The SLM process of the mixture of titanium and boron has many affecting factors some of which are unexpected or uncontrollable. As is shown in Figure 1.2, these factors are roughly categorized as: laser related, material related, reaction related, and other factors.

For the laser related factors, laser power and scanning speed are the two major parameters that can be controlled by design. Different values can also be assigned to change the focus diameter, scanning strategy, and hatch distance. Laser wavelength and beam profile are the

inherent attributes which cannot be changed. Gaussian distribution beam profile is simplified in this thesis.

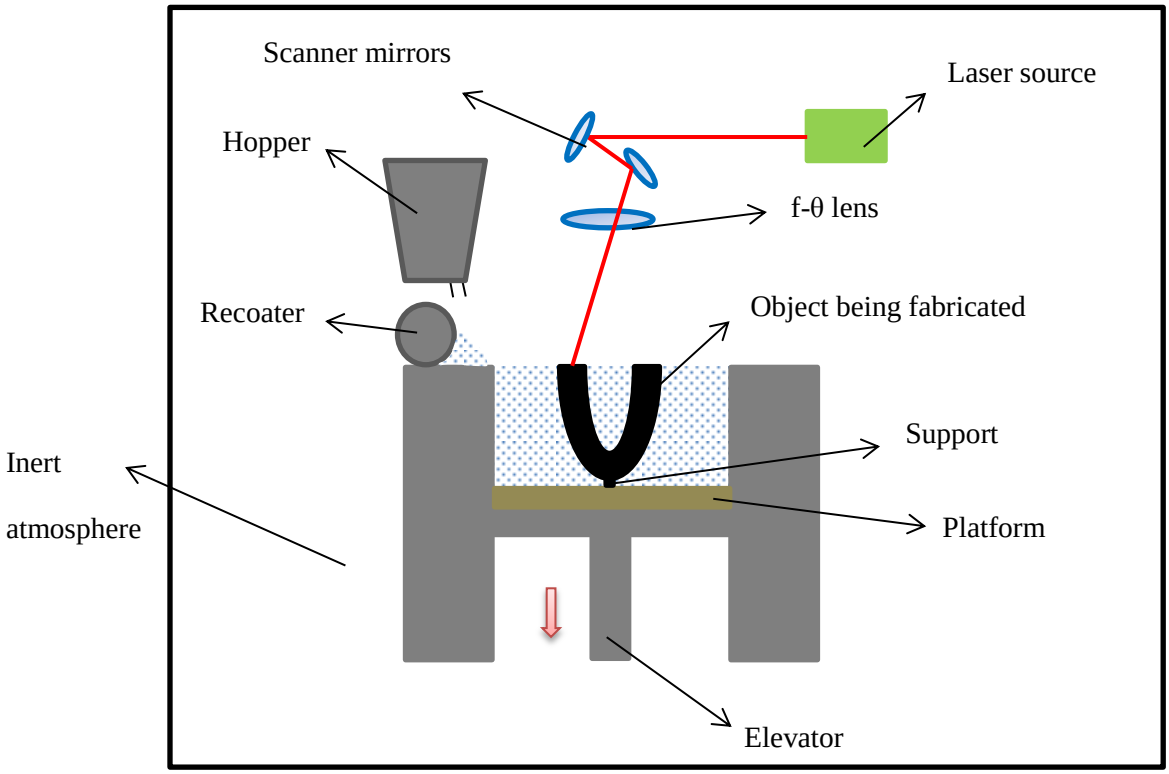

Figure 1.1 – Schematic overview of the SLM process

For the material related factors, different shapes, sizes, and molar ratios of titanium and boron display various physical and chemical properties, such as porosity, flowability, distribution, absorption of laser energy. The platform materials can be stainless steel, aluminum, titanium, ceramics, and so on. Different materials have different thermal properties (e.g. heat conductivity) which may significantly affect the SLM process. In addition, the existence of the unwanted elements can influence the analysis of the laser alloying procedures.

When it comes to the reaction related factors, the temperature-dependent properties of the powder system cannot be ignored. For example, the molar heat capacity of titanium and boron

increases with the increasing of temperature. The heat conductivity and laser energy absorption can be different with different temperatures. To control the reaction between titanium and boron, the reaction trigger temperature is a critical temperature that needs analyzing. Energy dissipation while reaction is almost an unmeasurable factor which depends on not only the type of reaction, but also the surrounding environment.

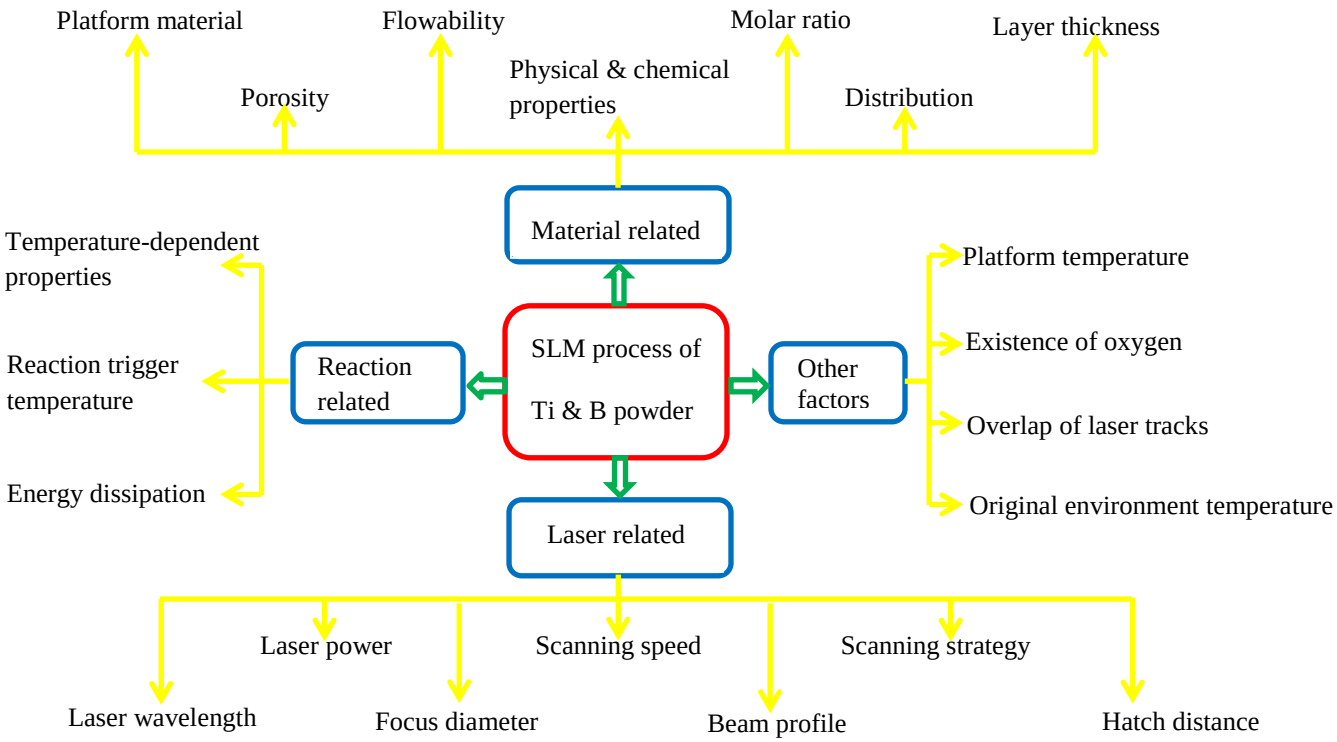

Figure 1.2 – Affecting factors on the SLM processing of titanium and boron

Besides the factors mentioned above, there are still a lot of other factors that matter. The platform temperature supplied by RENISHAW is adjustable which can be raised up to 170^{o}C. The existence of oxygen is unavoidable while preparing the starting powder and during the laser processing of the powder. Since oxygen can reaction with titanium, so it is important to manage

the oxygen in a very low level. If multiples lines or multiple layers need printing, the former lines or layers will affect the latter ones due to the former ones' residual heat and different surface morphologies. At last, the original environment temperature can also affect the process.

1.5 Organization of the Thesis

This thesis is arranged as follows: An introduction which discusses the significance of the selective laser alloying of the mixture of titanium and boron powder, the objectives need achieving and problems faced of this thesis is given in Chapter I; Chapter II provides a review of literature research includes topics of metallic alloying of elemental titanium and boron by different methods and models of SLM; In Chapter III, theoretical modeling of titanium and boron alloying process by SLM is developed and explained; Chapter IV described experimental work of the thesis. This includes variable values settlement, experiment design, preparation of the starting powder, experimental results, and verification of the theoretic models in Chapter III. Chapter V summarizes the findings of this thesis and also discusses the work that needs to be done in the future.

CHAPTER II

LITERATURE REVIEW

2.1 Overview of this Chapter

The first section of this chapter provides a review of the history of SLM, and its advantages over other additive manufacturing methods. The development of theoretic models of SLM is discussed in Section 2.3, which also points out that selective laser alloying process of titanium and boron powder is seldom studied. Section 2.4 reviews the traditional and laser-aided alloying methods of titanium and boron.

2.2 Selective Laser Melting

Compared to the traditional subtractive manufacturing of machining processes with metal removal, Additive manufacturing (AM, or 3D printing), used to make 3-dimensional (3D) objects, is a manufacturing process in which successive layers of material are laid down by having them designed under computer control. AM encompasses a wide variety of technologies for printing parts from 3D model, such as sintering and melting based processes. The original intend of selective laser sintering (SLS) process is to lower the cost and time of the product cycle design (Campanelli, Contuzzi, Angelastro, and Ludovico, 2010). This technology has been successfully applied to processing ceramics, plastic and metal powders. In order to bind the material together with the help of laser radiation to create a solid or porous structure, SLS sinters

or partially melts the powder bed. However, the unavoidable porosity of the parts created by the powder-liquid coexistence system of the laser sintering impedes its application to the functional metallic area, especially to the heavy-loading tasks. To solve this problem, another powder binding method – selective laser melting (SLM) was developed to obtain low porosity parts.

As one of the AM processes, SLM creates 3D metal parts by totally melting micron-scale metal powders together with the help of high-energy laser beam mounted inside the SLM machine. Different from classical SLS, SLM can achieve a homogenous part by fully melting the powder thanks for the higher laser energy adopted, not just fusing the powder together. Mumtaz et al. fabricated Waspaloy specimens with 99.3% dense by optimizing processing parameters of SLM (Mumtaz, Hopkinson, and Erasenthiran, 2008). Similarly, the almost fully dense (>99.5%) Ti-TiB_2 composites were obtained by Attar et al. (Attar, Bönisch, Calin, Zhang, Scudino, and Eckert, 2014). And usually, additional material with lower melting point, as is the case with SLS, is not a necessity for SLM. The major types of materials that can be processes by SLM are a wide range of metals and their alloys, such as stainless steel, aluminum, cobalt chrome, and titanium (Brodin, Andersson, and Johansson, 2013).

As the most effective powder based AM method (Gebhardt, Schmidt, Hötter, Sokalla, and Sokalla, 2010), SLM gains its popularity in the medical and aerospace area. On account of limitations of traditional manufacturing method, the ability of SLM to build lightweight and net shape parts is of great importance for aerospace engineering (Gini, 2012). Owing to its complete freedom of defining the geometry of parts (Kruf, Van de Vorst, Maalderink, and Kamperman, 2006), SLM has been widely used to the cellular/porous structures creation (Campanelli, Contuzzi, Angelastro, and Ludovico, 2010).

2.3 Theoretic Models of SLM

Theoretic models of SLM can be used to predict physical phenomena, such as melting and evaporating, and can also contribute to determining proper processing parameters of the manufacturing process (Zeng, Pal, and Stucker, 2012). An one-dimensional melting problem of laser irradiation on a semi-infinite powder bed was analytically solved by Zhang et al (Zhang, and Faghri, 1999). And they also numerically simulated a two-dimensional melting process on the powder bed with the Gaussian-distributed moving laser beam (Zhang, and Faghri, 1998). Taking convection and surface tension effect into consideration, Kou et al. developed a three-dimensional model to investigate the laser melted pool (Kou, and Wang, 1986). As usual, the Fourier heat conduction theory with heat transfer equations is utilized to model the laser energy input and thermal evolution of the powder bed (Carslaw, and Jaeger, 1959). Instead of Gaussian-distributed profile of laser beam, an axisymmetric heat conduction problem which assumed an uniform laser beam was solved to investigate the melting of Cu with a pulsed laser source (Shiomi, Yoshidome, Abe, and Osakada, 1999). Nevertheless, very few researches have been done on the selective laser alloying of the mixture of two different powders, especially when taking the reaction between those two powders into account. This thesis has put forward theoretic models of selective laser alloying of elemental titanium and boron with the consideration of reaction between them.

2.4 Titanium and Boron Alloying Methods

Taking the safety requirement into account, metallic biomaterials of high strength and toughness, such as stainless steel, Co-Cr alloys, CP Ti and its alloys, are extensively used for implants (Li, Yang, Zhao, Qu, Li, and Li, 2014). CP Ti and its alloys win over their competing

metallic biomaterials because of their better biocompatibility and corrosion resistance when it comes to biomedical applications (Long, and Rack, 1998). High wear resistant, high elastic impedance and high compressive strength make the Ti-B alloys the ideal candidate for their applications of armored vehicles (Wang, and Thompson, 1999).

Conventional cast metallurgy approach and powder metallurgy technique can be used to produce Ti-B alloys (Tamirisakandala, Miracle, Srinivasan, and Gunasekera, 2006). By adding boron powder into the titanium sample which would be melted in a small arc furnace under an inert gas atmosphere, Ti-B alloys with different elements ratios, such as Ti-0.05B and Ti-0.1B were casted (Bermingham, McDonald, Nogita, John, and Dargusch, 2008). And it was founded that trace additions of boron refined the α–grain size in CP titanium, which significantly affected the microstructure of titanium. Tamirisakandala et al. reduced the grain size of as-cast Ti-6Al-4V from 1700 to 200 μm with 0.1 wt.% boron addition which is roughly an order of magnitude (Tamirisakandala, Bhat, Tiley, and Miracle, 2005). The pre-alloyed powder metallurgy of gas-atomizing Ti-6Al-4V and boron was adopted to produce Ti-B alloy with uniform and fine dispersions of TiB (Yolton, 2004). Wang et al. fabricated TiB_2 ceramic disks with density above 98% by using the self-propagating high-temperature synthesis/dynamic consolidation (SHS/DC) method (Wang, and Thompson, 1999). The disks' structural and mechanical properties were adjusted to satisfy military and civilian demands. The spark plasma sintering method was performed by Schmidt et al. who mixed the commercial Ti and amorphous B powders with a molar ratio of Ti:B=1:2 in a swing mill. Then, they applied the pulsed high dc current and load to these as-starting powders to create needle-shaped TiB_2 (Schmidt, Boehling, Burkhardt, and Grin, 2007).

In addition to these traditional approaches of producing Ti-B alloys mentioned above, laser-aided methods are widely used, especially when it comes to surface hardening of titanium. For the physical property demanding area, such as aerospace and other advanced field, discontinuously reinforced titanium-titanium boride (Ti-TiB) composites gain their popularity (Ravi Chandran et al., 2004, Chandrasekar et al., 2007, Makuch et al., 2014). Laser surface alloying with boron on CP titanium was carried out to create laser-borided layer with the help of continuous-wave CO_2 laser (Makuch, Kulka, Dziarski, and Przestacki, 2014). The formation of the laser-borided surface layer substantially enhances the corrosion resistance, stiffness, wear resistance and microhardness of the CP titanium. Chandrasekar et al. applied 10 kW CO_2 laser system on the Ti-TiB composite of titanium matrix with 34 vol.% of TiB whiskers. Compare to the untreated titanium surface, a dramatical increase of surface hardness from 513 VHN to 1055 VHN could be the observed (Chandrasekar, Balusamy, Ravi Chandran, and Kumar, 2007). The laser-aided methods win over the conventional diffusion surface treatment method since the latter method always takes a long processing time and demands a high processing temperature. Taking the complex-shape parts creation into consideration, SLM is a speedy manufacturing process. Attar et al. fabricated almost fully dense (>99.5%) Ti-TiB composites by tuning the SLM manufacturing parameters on the optimally milled Ti-TiB_2 powder (Attar, Bönisch, Calin, Zhang, Scudino, and Echert, 2014).

Selective laser alloying process of elemental titanium and boron by SLM machine has been analyzed in this thesis. The reaction equations between titanium and boron are:

$$\mathrm{Ti} + 2\mathrm{B} \rightarrow \mathrm{TiB_2} \quad \Delta G(\mathrm{R}, 1000\mathrm{K}) = -308\ \mathrm{kJ/mol} \tag{1}$$

$$\mathrm{Ti} + \mathrm{TiB_2} \rightarrow 2\mathrm{TiB} \quad \Delta G(\mathrm{R}, 1000\mathrm{K}) = -6.3\ \mathrm{kJ/mol} \tag{2}$$

$$T_i + B \rightarrow T_iB \quad \Delta G(R, 1000K) = -157\ kJ/mol \tag{3}$$

The negative values of ΔG (the Gibb free energy), calculated by using the thermodynamic data (Barin, 1995), of the reactions above indicate that they are exothermic reactions.

CHAPTER III

RESEARCH METHODOLOGY

3.1 Overview of this Chapter

Different laser energy input, which can be controlled by adjusting SLM process parameters, will arouse several important physical and chemical phenomena between the titanium and boron powder system, such as the melting and evaporating of titanium, boron and their alloys, reactions between titanium, boron and their alloys. In turn, the energy generated from the reaction will affect the alloying process. This chapter focuses on the models creation of different laser energy input on the titanium and boron powder system. Molar ratio between the titanium and boron is another important factor which is also discussed in this chapter.

3.2 Theoretic Models of General Selective Laser Alloying of Titanium and Boron

For SLM machine, laser is the most important heat source. The heatable substrate of AM250 laser melting machine from RENISHAW company can be another heat source. And as mentioned before, the reactions between titanium and boron can release a huge amount of energy which can also be a heat source if the reactions are triggered. The energy that can be utilized by the titanium and boron system is descripted as follows:

$$E_{in} - E_{out} = E_{system} \quad (4)$$

Here, E_{in} designates the total energy generated from the process, including laser energy and the energy released from the reaction; E_{out} designates the energy escaped out of the system, such as the reflection of laser energy, the heat irradiation to the surrounding area and so on; E_{system} designates the effective energy that can be absorbed by the powder system.

Thus, Equation (4) can be rewritten as:

$$E_{laser} + E_r - E_{laser\_reflection} - E_{r\_dissipation} = E_{system} \quad (5)$$

$$E_{laser\_absorption} + E_{r\_absorption} = E_{system} \quad (6)$$

Where, $E_{laser\_absorption} = AE_{laser}$, A is the absorption coefficient of opaque metal surface of the powder bed. It can be concluded that the combination of the absorption of laser energy ($E_{laser\_absorption}$) and the absorption of the energy from the reaction ($E_{r\_absorption}$) is the total energy that can be used by the system.

Since the elemental titanium and boron can form different compounds, such as TiB, Ti_3B_4, TiB_2 and so on, several models have been developed based on different molar ratios between titanium and boron.

$$T_i : B = 1 : x$$

$$\begin{cases} T_i + 2B \rightarrow T_iB_2, \quad \Delta G(T_iB_2) & 1:x \leq 1:2 \\ T_i + B \rightarrow T_iB, \quad \Delta G(T_iB) & 1:x \geq 1:1 \\ T_i + xB \rightarrow (x-1)T_iB_2 + (2-x)T_iB, \quad (x-1)\Delta G(T_iB_2) + (2-x)\Delta G(T_iB) & 1:2 < 1:x < 1:1 \end{cases}$$

3.2.1 Molar ratio of Ti:B≤1:2

The first case is when the boron is excessive. To develop a general model, it is assumed that the energy that can be used by the powder system is high enough to allow all the physical and chemical phenomena to happen (Yshida, Kobashi, Kanetake, 2007).

$$E_{system} = n_{T_i}\int_{T_o}^{T_R}\left[c_p(T_i) + 2c_p(B)\right]dT + \left(n_B - 2n_{T_i}\right)\left[\int_{T_o}^{T_F} c_p(B)dT + L_l(B) + L_v(B)\right] + n_{T_iB_2}\left[\int_{T_R}^{T_F} c_p(T_iB_2)\,dT + L_l(T_iB_2) + L_v(T_iB_2)\right] \quad (7)$$

Here, n_{T_i}, n_B, and $n_{T_iB_2}$ denote amount of substance of titanium, boron, and titanium diboride, respectively; $c_p(T_i)$, $c_p(B)$ and $c_p(T_iB_2)$ are the molar heat capacity of titanium, boron, and titanium diboride; $L_l(B)$ and $L_l(T_iB_2)$ indicate the latent heat of liquefaction of boron and titanium diboride; Similarly, $L_v(B)$ and $L_v(T_iB_2)$ indicate the latent heat of vaporization of boron and titanium diboride; T_o is the original temperature of the powder system; T_R denotes the reaction trigger temperature; T_F is the final temperature of the powder system.

The reaction trigger temperature T_R (around 450 ^oC) is lower than all the elements and compounds' melting temperature (Schmidt, Boehling, Burkhardt, and Grin, 2007). $\int_{T_o}^{T_F} c_p(B)dT$ can be expanded as $\int_{T_o}^{T_R} c_p(B)dT + \int_{T_R}^{T_F} c_p(B)dT$. It is known that the molar ratio between titanium and boron is $1:x$. If $n_{T_i} = n$, $n_B = xn$ and $n_{T_iB_2} = n$. So, Equation (7) can be simplified as:

$$\frac{E_{system}}{n} = \int_{T_o}^{T_R}\left[c_p(T_i) + xc_p(B)\right]dT + (x-2)\left[\int_{T_R}^{T_F} c_p(B)dT + L_l(B) + L_v(B)\right] + \int_{T_R}^{T_F} c_p(T_iB_2)\,dT + L_l(T_iB_2) + L_v(T_iB_2) \quad (8)$$

3.2.2 Molar ratio of Ti:B≥1:1

The over dose of titanium leads to different laser processing and reactions between titanium and boron. Based on Equation (3), the model of this case is described as follows:

$$E_{system} = n_B \int_{T_o}^{T_R} \left[c_p(T_i) + c_p(B)\right] dT + \left(n_{T_i} - n_B\right) \left[\int_{T_o}^{T_F} c_p(T_i) dT + L_l(T_i) + L_v(T_i)\right] + n_{T_iB} \left[\int_{T_R}^{T_F} c_p(T_iB)\, dT + L_l(T_iB) + L_v(T_iB)\right] \quad (9)$$

Here, symbols of Equation (9) share the same meaning of Equation (7) but T_R. The T_R of Equation (7) denotes the trigger temperature of Equation (1), while the T_R of Equation (9) denotes the trigger temperature of Equation (3). In addition, n_{T_iB}, $c_p(T_iB)$, $L_l(T_iB)$, and $L_v(T_iB)$ indicate TiB's amount of substance, molar heat capacity latent heat of liquefaction, and latent heat of vaporization. If $n_{T_i} = n$, $n_B = xn$ and $n_{T_iB_2} = xn$. So, Equation (9) can be simplified as:

$$\frac{E_{system}}{n} = x \int_{T_o}^{T_R} c_p(B)\, dT + \int_{T_o}^{T_R} c_p(T_i)\, dT + (1-x) \left[\int_{T_R}^{T_F} c_p(T_i) dT + L_l(T_i) + L_v(T_i)\right] + x \left[\int_{T_R}^{T_F} c_p(T_iB)\, dT + L_l(T_iB) + L_v(T_iB)\right] \quad (10)$$

3.2.3 Molar ratio of 1:2 <Ti:B<1:1

Assume that if the molar ratio of titanium and boron is between the two critical values 1:2 and 1:1, the following reaction will occur:

$$T_i + xB \rightarrow (x-1)T_iB_2 + (2-x)T_iB, \quad (x-1)\Delta G(T_iB_2) + (2-x)\Delta G(T_iB)$$

Then, the model of this case is:

$$E_{system} = \int_{T_o}^{T_R} \left[n_{T_i} c_p(T_i) + n_B c_p(B) \right] dT + n_{T_iB_2} \left[\int_{T_R}^{T_F} c_p(T_iB_2)\, dT + L_l(T_iB_2) + L_v(T_iB_2) \right] + n_{T_iB} \left[\int_{T_R}^{T_F} c_p(T_iB)\, dT + L_l(T_iB) + L_v(T_iB) \right] \quad (11)$$

If $n_{T_i} = n$, then $n_B = xn, n_{T_iB_2} = (x-1)n$, $n_{T_iB} = (2-x)n$. Equation (11) can be simplified as:

$$\frac{E_{system}}{n} = \int_{T_o}^{T_R} \left[c_p(T_i) + x c_p(B) \right] dT + (x-1) \left[\int_{T_R}^{T_F} c_p(T_iB_2)\, dT + L_l(T_iB_2) + L_v(T_iB_2) \right] + (2-x) \left[\int_{T_R}^{T_F} c_p(T_iB)\, dT + L_l(T_iB) + L_v(T_iB) \right] \quad (12)$$

However, since the trigger temperature T_R of the formation of TiB_2 and TiB is not one same value, the model has to be modified to compensate the difference. At the same time, within this ratio scale, the possibility of the formation of Ti_3B_4 will further complicate this case. Although we developed the model for Ti_3B_4, due to its limitation, this thesis will focus on Ti:B=1:2 and Ti:B=4:1 only.

3.2.4 Volumetric selective laser alloying zone on the powder bed

The volumetric heat source is adopted in this thesis work since the laser energy is deposited in the bulk of the powder bed instead of just on the top surface (Gusarov, Yadroitsev, Bertrand, and Smurov, 2009). The reason is that the laser beam can be reflected several times until it reaches a certain depth (Wang et al., 2002).

Mazumder et al treated the laser beam as a heat flux, Q, which is a Gaussian-distributed heat source (Mazumder, and Kar, 1995). And the heat flux is in proportion to the laser power, P. It can be described as:

$$Q = \frac{2PA}{\pi r_0^2} e^{-\frac{2r^2}{r_0^2}} \tag{13}$$

Where r_0 is the radius of the laser beam which is demonstrated in Figure 3.1. The r_0 is chosen the value of which is e^{-2} times of that of the central laser beam. And r is the distance between the point of the powder bed surface and the center point. The real laser beam has a Gaussian distribution profile, while the vicinity of the beam focus is similar to a top-hat profile (Kaplan, 2011).

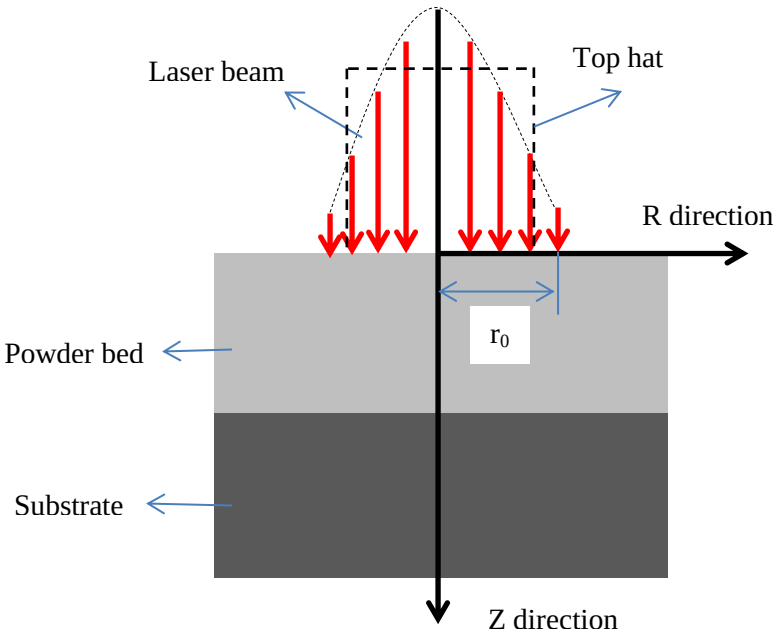

Figure 3.1 – The Gaussian distribution laser power on the powder bed

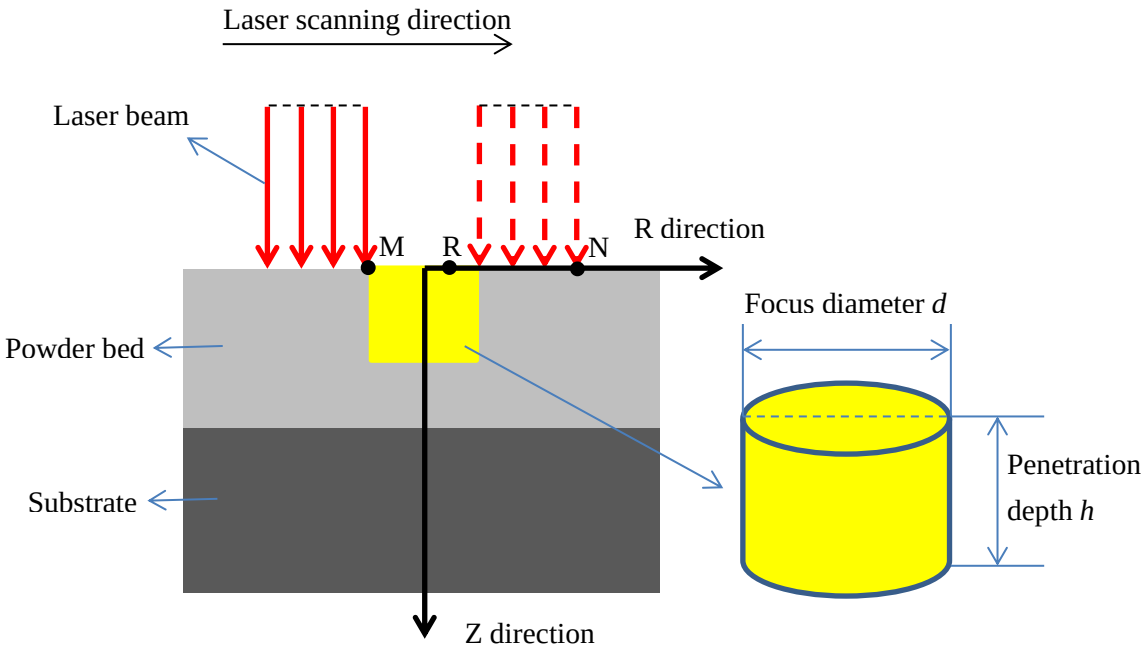

Figure 3.2 – The detailed volumetric heat source of the laser and powder bed contact zone

It can be seen from Figure 3.2 that instead of Gaussian-distributed laser power, an R direction identically distributed laser powder is adopted to simplify the model in this thesis. The collimated incident beam penetrates into the powder evenly along the Z direction. Therefore, the volumetric laser alloying zone is a cylinder with the diameter d (the same as laser's focus diameter) and height h (laser penetration depth). Suppose that the laser scanning speed is v, laser scanning from point M to point N with the distance of 2d would take the time of 2d/v. Because a point on the yellow surface area R is exposed to the laser beam for a duration of d/v, the whole cylinder is exposed under the laser beam for a duration of d/v, too. It means that the laser irradiation time of a certain area is d/v. P is the power of laser with the unit of watts. Then, $E_{laser-absorption}$ of Equation (6) is:

$$E_{laser\_absorption} = AE_{laser} = APt = APd/v \tag{14}$$

A denotes the laser absorption coefficient of the powder system with titanium and boron. Tolochko et al. calculated the absorption of a powder mixture of two components by using the following equation (Tolochko, Khlopkov, Mozzharov, Lgnatiev, Laoui, and Titov, 2000):

$$A = A_1\gamma_1 + A_2\gamma_2 \tag{15}$$

Here, A_i and γ_i indicate the absorption coefficient and volume fraction of component i, respectively.

The reaction absorption energy is:

$$\frac{E_{r\_absorption}}{n} = A'|\Delta G| \tag{16}$$

Similarly, A' denotes the reaction absorption coefficient of the powder bed; $|\Delta G|$ is the absolute value of the energy released from the reaction.

Due to the multi-reflection of the laser beam, the laser radiation can penetrate into the powder bed of a certain depth h. Here, we assume that within the height of h, the laser powder is identically distributed, and beyond the height of h, there is no laser energy. The volume of this cylinder is:

$$V = \pi\left(\frac{d}{2}\right)^2 h \tag{17}$$

It is known that the molar ratio between titanium and boron is $1:x$. Then, the amount of titanium can be calculated as follows:

$$V_{T_i}:V_B = \frac{m_{T_i}}{\rho_{T_i}}:\frac{m_B}{\rho_B} = \frac{n_{T_i}M_{T_i}}{\rho_{T_i}}:\frac{n_B M_B}{\rho_B} \tag{18}$$

$$m_{T_i} = \rho_{T_i} \frac{V_{T_i}}{V_{T_i} + V_B} V(1 - \varepsilon) \tag{19}$$

Hence,

$$n = n_{T_i} = \frac{m_{T_i}}{M_{T_i}} = \frac{\pi d^2 h \rho_{T_i} \rho_B (1 - \varepsilon)}{4\left(\rho_B M_{T_i} + x \rho_{T_i} M_B\right)} \tag{20}$$

Here, $m_{T_i}$and m_B denote the mass of titanium and boron, respectively; $V_{T_i}$and $V_B$are the volume; ρ_{T_i} and ρ_B denote the density of titanium and boron; $M_{T_i}$and M_B are titanium's and boron's molar mass, respectively; ε designates the porosity of the powder bed.

So,

$$\frac{E_{system}}{n} = \frac{E_{laser\_absorption} + E_{r\_absorption}}{n}$$

$$= \frac{4\left(\rho_B M_{T_i} + x \rho_{T_i} M_B\right)\left(A_{T_i} \gamma_{T_i} + A_B \gamma_B\right) Pd}{v \pi d^2 h \rho_{T_i} \rho_B (1 - \varepsilon)} + A' |\Delta G| \tag{21}$$

CHAPTER IV

EXPERIMENTAL STUDY AND RESULT ANALYSIS

4.1 Overview of This Chapter

To fully understand the selective laser alloying process of titanium and boron powder, the newly developed theoretic models are used to assist in interpreting the related experiment results. It is proved that these models are in good agreement with experiment results. The flowchart shown in Figure 4.1 can briefly illustrate the logic structure of this chapter.

The flowchart starts with the theoretic models developed in Chapter III. The values of the variables are settled in Section 4.2. Section 4.3 describes the design of experiment with the help of test series. Selective laser alloying on two different molar ratios of 1:2 and 4:1 between titanium and boron processes are discussed and analyzed. For the molar ratio of 1:2, low energy input and high energy input experiments are carried out separately. And the results from the low energy input experiment do help the analysis of high energy input experiment. For the molar ratio of 4:1, firstly, the contribution of reaction to the alloying process is proved by printing a few lines. This contribution can also be verified with the molar ratio of 1:2 which is shown in the flowchart. Secondly, the test series of single layers are printed to optimize the laser process parameters. Thirdly, the optimized parameters are utilized to build multiple layers with high surface quality. All the experiments can be treated as the verification experiments of the theoretic

models. In turn, the theoretic models contribute to understanding the selective laser alloying of reactive titanium and boron powder system.

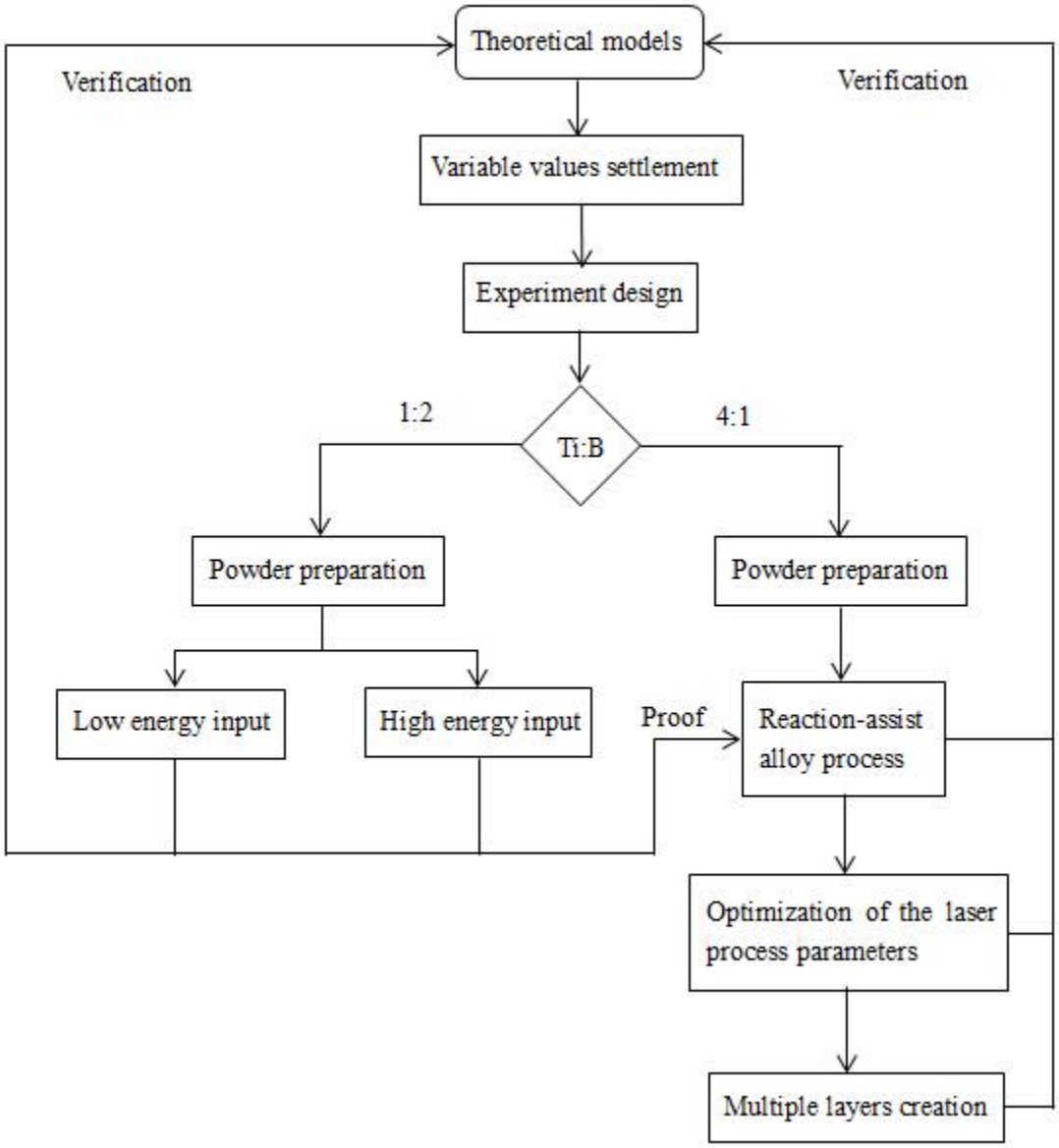

Figure 4.1 – Flowchart of the logic structure of this chapter

4.2 Process Parameters of Selective Laser Alloying of Ti-B System

The variables of the models correspondent to the process parameters of the selective laser alloying process, which can be categorized as laser related, titanium related, boron related, TiB_2 related, TiB related, reaction related and other factors.

For the laser related variables, the values are provided from the AM250 machine (RENISHAW) specification. The focus diameter of the laser beam is 70 μm; The maximum laser power of this machine is 200 W and can be adjusted from 0 to 200 W as needed; The maximum scanning speed of the laser is 7 m/s, and can be varied from 0 to 7 m/s; The penetration depth of the laser is the height of reaction area. Taking the fact that the laser power weakens rapidly along the Z direction (Figure 3.2), 50 μm which is shorter than the real penetration depth is adopted. In addition, 50 μm is also the suggested layer thickness of the machine; The absorption of the titanium powder by using Nd-YAG (λ=1.06 μm) laser is 0.77 (Tolochko et al., 2000). Since no absorption data of the boron is available, a constant conservative value of 50% is assumed regardless the volume ratio between titanium and boron.

The molar mass of titanium is 47.87 g/mol (Standard Atomic Weights, 2013), and all the other values are retrieved from industrial database (Titanium, 2015). Similarly, the molar mass of boron is 10.81 g/mol (Conventional Atomic Weights, 2013), and all the other values are retrieved from industrial database (Boron, 2015). The values are listed in Table 4.1.

The molar heat capacity of TiB_2 at the temperature of 300 K is 49.91 J/(mol·K) (Westrum, and Clay, 1978). And the latent heat of liquefaction of TiB_2 is 100.4 kJ/mol (Lide, 2009). The molar heat capacity of TiB ranges from 50.06 to 56.07 J/(mol·K) with the increasing of temperature from 700 K to 4000 K (Chase, 1998). A constant value of 51 J/(mol·K) is adopted

as TiB's molar heat capacity. The melting temperature of TiB_2 and TiB can be referred to Chapter I.

For the reaction related variables, the values of $\Delta G(T_iB_2)$ and $\Delta G(T_iB)$ obtained from Chapter II are under the temperature of 1000 K. Based on Matin et al.'s work, the ΔG of Equation (1) and Equation (3) at 298 K are -278 kJ/mol and -161 kJ/mol respectively, which means that the Gibb free energy does not change too much within narrow temperature range from 298 K to 1000 K (Matin, Lu, and Gupta, 2001). Thus, the approximate values of -300 kJ/mol and -160 kJ/mol for Equation (1) and Equation (3) will be adopted in this thesis.

$$\Delta G(T_iB_2) = -300\ \mathrm{kJ/mol}$$

$$\Delta G(T_iB) = -160\ \mathrm{kJ/mol}$$

It can be concluded that the formation of TiB_2 of Equation (1) is the most negative reaction. However, as long as the boron concentration in the reaction zone is less than 18 mass% (Feng, Meng, Zhou, and Jia, 2005), the further reaction between B and TiB_2 can take place because of the small negative ΔG value (Equation (2)).

When the reaction is on, most of the energy released will escape as light and heat, only a little bit of it can be captured by the surrounded powders. So the value of 10% is assigned to the reaction absorption coefficient. Schmidt et al. detected the exothermic reactions by raising the mixture of elemental titanium and boron powder with the molar ratio of 1:2 to 450^{o}C. So, the trigger temperature of the reaction $T_i + 2B \rightarrow T_iB_2$ is 723K. If the molar ratio between titanium and boron is 4:1, the reaction $T_i + B \rightarrow T_iB$ takes place as two steps as shown in Equations (1) and (2). The Equation (1) occurs first. Due to the negative ΔG value, Equation (2) will also happen soon afterwards. Thus, the trigger temperature of the reaction $T_i + B \rightarrow T_iB$ can also be

considered as 723K. Room temperature of 298 K is the original temperature of this system. The porosity of 40% is selected based on the powders shape and compact condition.

It should be noticed that some of the properties are temperature-dependent, such as density, laser absorption coefficient, and molar heat capacity. So, errors cannot be avoided.

Table 4.1 – Variable values

Categories	Variables	Values
Laser related	Focus diameter: d (μm)	70
	Laser power: P (W)	0-200
	Scanning speed: v (m/s)	<7
	Penetration depth: h (μm)	50
	Laser absorption coeff.: A	50%
Titanium related	Molar mass: M_{T_i} (g/mol)	47.87
	Density: ρ_{T_i} (g/cm^3)	4.51
	Molar heat capacity: $c_p(T_i)$ $(J/(mol \cdot K))$	25.06
	Latent heat of liquefaction: $L_l(T_i)$ (kJ/mol)	14.15
	Latent heat of vaporization: $L_v(T_i)$ (kJ/mol)	425
	Melting temperature: $T_M(T_i)$ (K)	1941
	Boiling temperature: $T_B(T_i)$ (K)	3560
Boron related	Molar mass: M_B (g/mol)	10.81
	Density: ρ_B (g/cm^3)	2.08
	Molar heat capacity: $c_p(B)$ $(J/(mol \cdot K))$	11.09
	Latent heat of liquefaction: $L_l(B)$ (kJ/mol)	50.2
	Latent heat of vaporization: $L_v(B)$ (kJ/mol)	508
	Melting temperature: $T_M(B)$ (K)	2349
	Boiling temperature: $T_B(B)$ (K)	4200
	Molar heat capacity: $c_p(T_iB_2)$ $(J/(mol \cdot K))$	49.91

T_iB_2 related	Latent heat of liquefaction: $L_l(T_iB_2)$ (kJ/mol)	100.4
	Latent heat of vaporization: $L_v(T_iB_2)$ (kJ/mol)	/
	Melting temperature: $T_M(T_iB_2)$ (K)	3243
	Boiling temperature: $T_B(T_iB_2)$ (K)	/
T_iB related	Molar heat capacity: $c_p(TB_i)$ (J/(mol · K))	51
	Latent heat of liquefaction: $L_l(T_iB)$ (kJ/mol)	/
	Latent heat of vaporization: $L_v(T_iB)$ (kJ/mol)	/
	Melting temperature: $T_M(T_iB)$ (K)	2473
	Boiling temperature: $T_B(T_iB)$ (K)	/
Reaction related	Reaction released energy: $\Delta G(T_iB_2)$ (kJ/mol)	-300
	Reaction released energy: $\Delta G(T_iB)$ (kJ/mol)	-160
	Reaction absorption coeff.: A'	10%
	Reaction trigger temperature: T_R (K)	723
Other	Original temperature (Room temp.) (K)	298
	Porosity: ε	40%

4.3 Experiment Design

To save time and material, different processing parameters can be tested at the same time by creating test series. In practice, 4 values of Parameter I and Parameter II are assigned along the X and Y directions as is shown in Figure 4.2. Thus, 4×4=16 samples can be created at one time for the following analysis. In this thesis, two types of melting mechanisms are investigated: melting on the solid substrates (stainless steel and ceramics); and melting on the loose powder cavities (aluminum).

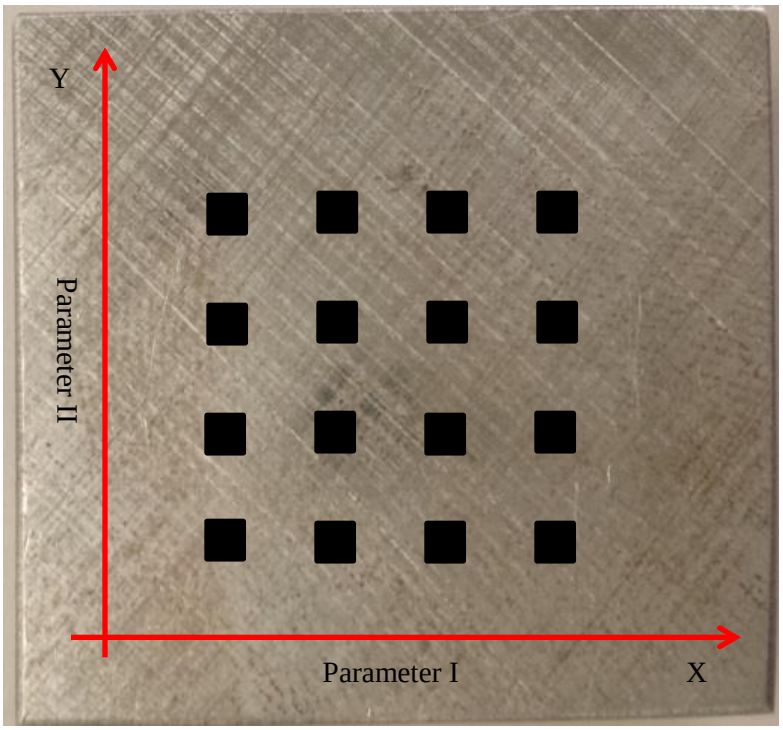

(a)

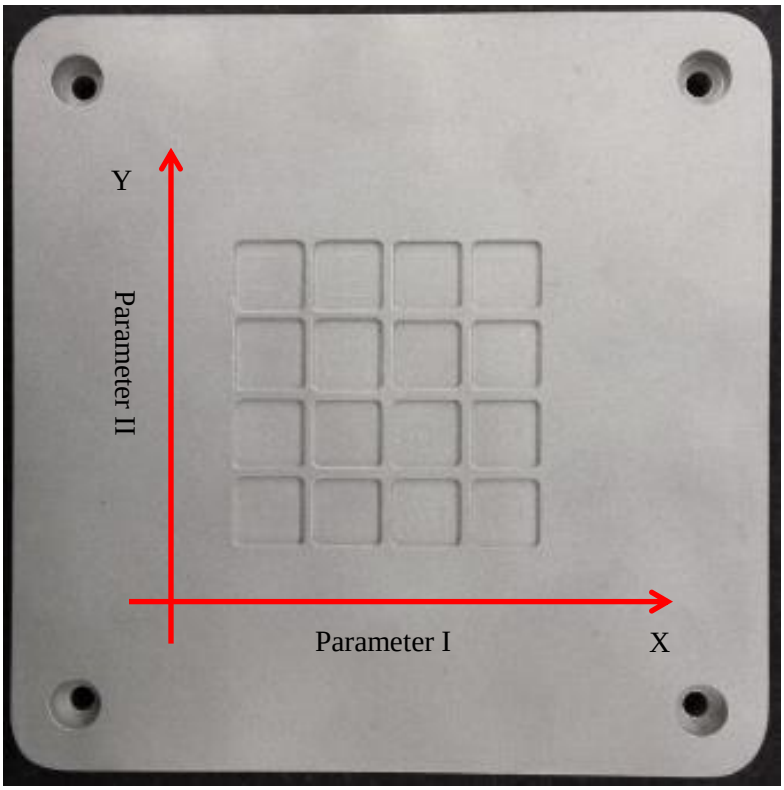

(b)

Figure 4.2 – (a) Solid substrate made of stainless steel, and (b) loose powder substrate made of aluminum

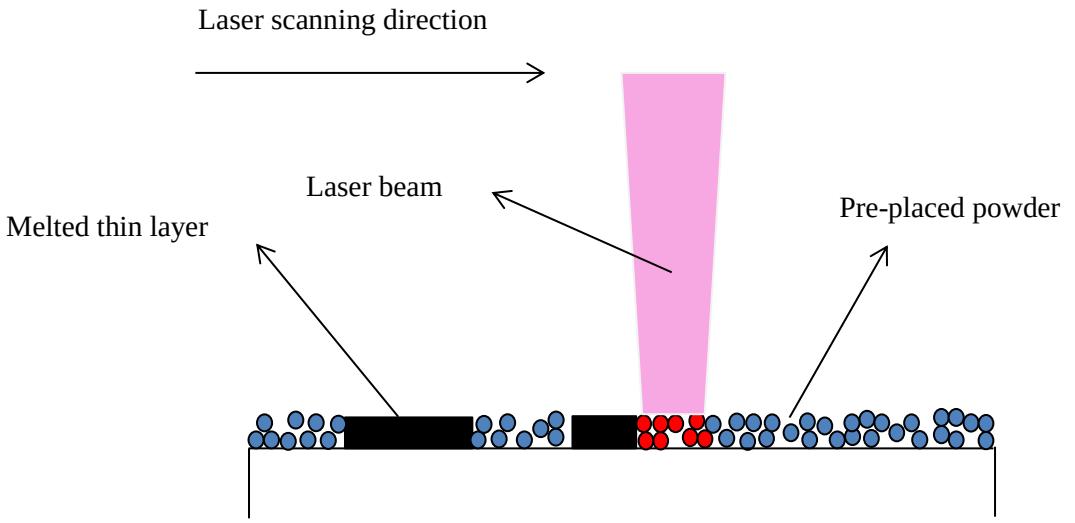

(a)

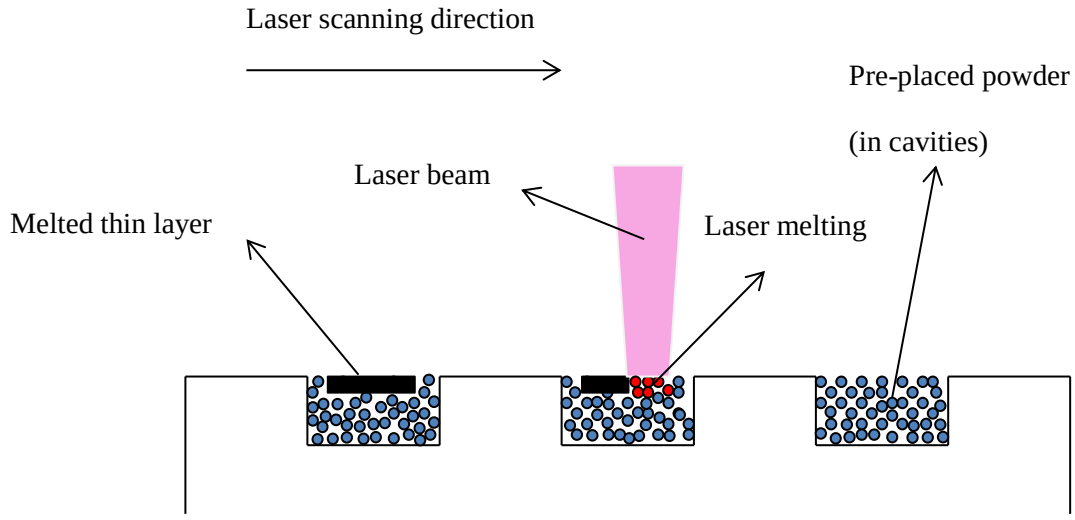

(b)

Figure 4.3 – Schematic overview of the two types of melting mechanisms: (a) melting on the solid substrate; (b) melting on the loose powder

Figure 4.2a shows the stainless steel solid substrate on which layers of testing powders can be printed. Since iron is also easily melted, the stainless steel solid substrate may affect the printed layers of testing powders by adding iron element, especially when only a few layers are printed. In this case, ceramics solid substrate will be used instead to avoid the effect of stainless steel substrate. For the aluminum substrate with 16 cavities on the top surface, the laser processes the powder on the top layer of the cavities. Since the cavities have relatively deep depth of 0.8 mm, compare to the 50 μm printing layer, the effect of the substrate on the printing process is small enough to be eliminated.

As can be seen from Figure 4.2a and Figure 4.3a, the melted thin layer is attached to the solid substrate. While for Figure 4.2b and Figure 4.3b, the melted thin layer on top of the loose powder can be removed easily for post-processing.

4.4 Powder Preparation

4.4.1 Powder properties

The commercial pure (CP) Ti powder (Figure 4.4a) with spherical shape supplied by LPW Technology Ltd. (USA) was used in this thesis. The normal particle size distribution is between 15 to 45 microns. Table 4.2 shows the chemical composition of the powder (wt. %). It can be seen that the boron powder, supplied by the Chemsavers. Inc. (USA), exhibits an irregular shape (Figure 4.4b), whose purity is greater than 96%. And the boron powder's particle size is less than 5 microns.

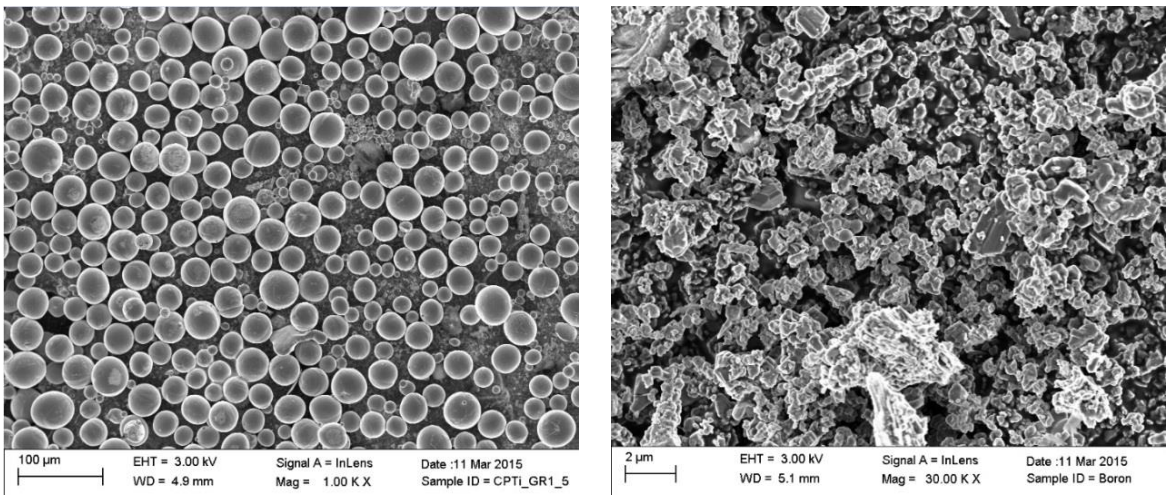

(a) **(b)**

Figure 4.4 – Scanning electron microscope (SEM) images of shape and morphology of the powders in as-received condition: (a) CP Ti, and (b) B (<5 micron)

Table 4.2 – Chemical compositions (wt. %) of the CP Ti powder

Element	C	Fe	H	N	O	Ti
Content (wt. %)	0.08	0.20	0.015	0.03	0.18	Balance

4.4.2 Mechanical alloy process

The mechanical mixing of the elemental powders (Ti and B) was carried out by using the planetary ball mill PM 200 (Retsch, Germany) under the protective argon atmosphere. Two different molar ratios of Ti:B=1:2 (Ti-31 wt.% B) and Ti:B=4:1 (Ti-5.3 wt.% B) were processed. Ball (steel balls with diameter of 10 mm) to powder weight ratio of 5:1 was adopted in this thesis. To avoid alloy or reaction between Ti and B powders, a relatively low rotation speed of 100 rpm for 1~3 hours was set for the ball milling process. And the machine would rest for 10 seconds every 5 minutes.

4.4.3 Microstructural characterization

Phase characterization identification was performed with powder X-ray diffraction (XRD) (Bruker D8 Advanced XRD Instrument). The wide range of $2\theta=10\sim100^{o}$ with a continuous scan mode was carried out to generate a general information of the diffraction peaks. Compare the XRD experiment results with the existing substances database of XRD, phase composition can be determined if the experiment diffraction peaks match the corresponding peak positions from the database. The SEM machine enabled the observation of microstructures of the samples with the resolution up to 1 nm. The surface shape morphology and size distribution of the material to be observed can be provided. Energy-dispersive X-ray spectroscopy (EDAX), integrated within the SEM machine, can identify and quantify the elements to be observed.

4.5 Verification Experiments

4.5.1 Powder preparation results and discussion

Figure 4.5 shows the mixing condition and particle-morphologies of the Ti-B powders after different times of milling. During the milling process, spherical titanium particles were distributed among the finer irregular boron powders and some of the titanium powders were formed into rod shape. While, cavities were created due to the loose density of the as-received boron powder as is shown in Figure 4.5c.

After the first hour of milling, the titanium particles were not uniformly distributed among the boron matrix (Figure 4.5a). The yellow-dash circled area contained very few titanium particles. Compare to the cavities shown in Figure 4.5b, the cavities of Figure 4.5a were relatively smaller but deeper. For Figure 4.5b, the titanium particles were well distributed among the boron matrix, without obvious “blank area” circled by yellow dashed lines as shown in

Figure 4.5a. In addition, the shallow cavities which slightly affected the selective laser alloying process of Figure 4.5b were acceptable. By increasing the milling time to 3 h (Figure 4.5c), the cavities became deeper. And the titanium particles were preferentially dispersed into these cavity areas. Because of long time of milling, the collisions between balls and powders flattened the titanium particles into rod shape (Figure 4.5c). According to the above, 2 h ball milling of the Ti-B was selected as the optimizing process parameter of the starting powder for SLM due to the well-distributed titanium powder among boron matrix and the relatively shallow cavities. In addition, the titanium particles maintained spherical shape.

Figure 4.6 shows the XRD pattern of Ti-B ball-milled for 2 h. It can be seen that there are only elemental titanium and boron after the milling. No diffraction peaks of TiB or TiB_2 were observed which satisfied our experiment purpose. In another word, mechanical mixing, instead of mechanical alloy, of the titanium and boron powders were created for the following SLM processes.

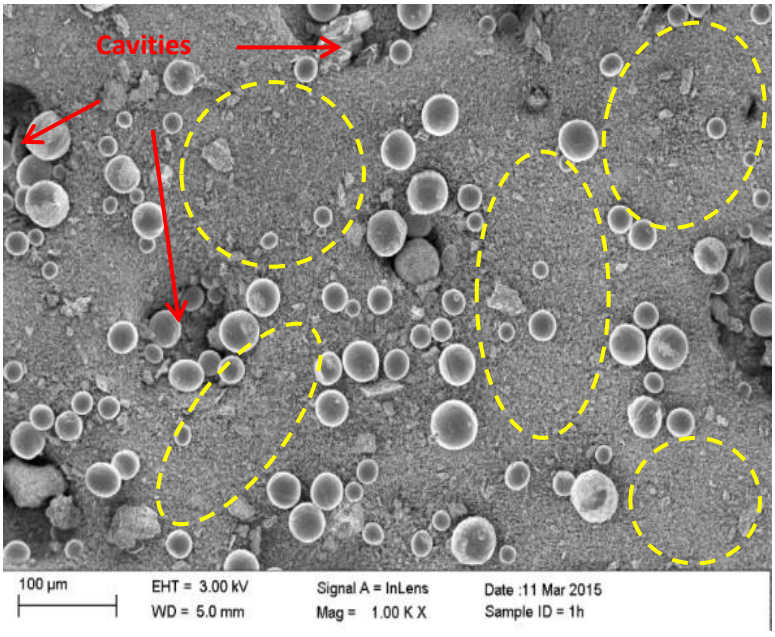

(a)

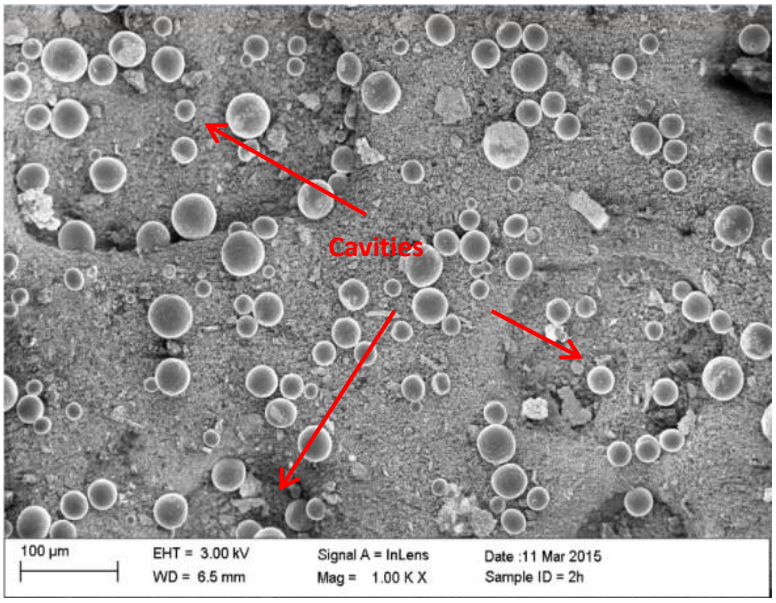

(b)

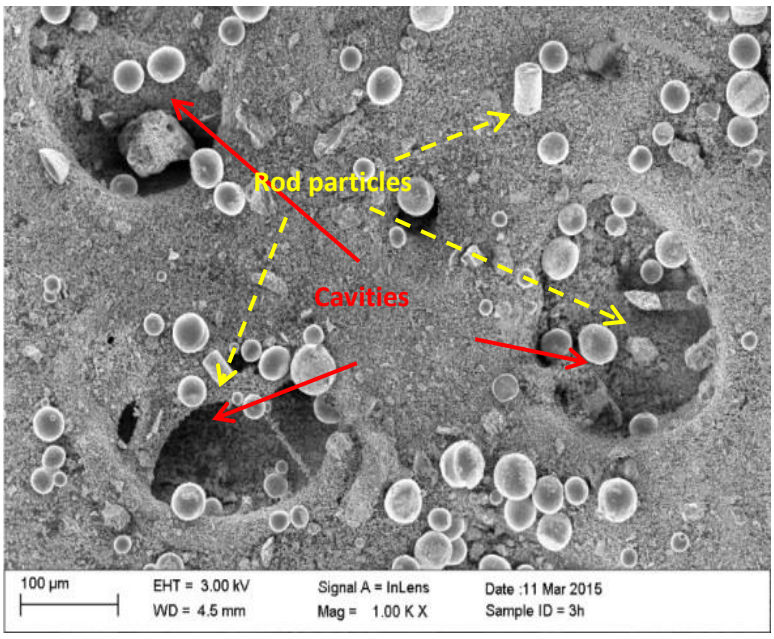

(c)

Figure 4.5 – SEM images of Ti-B powders ball-milled for (a) 1h, (b) 2h, and (c) 3h

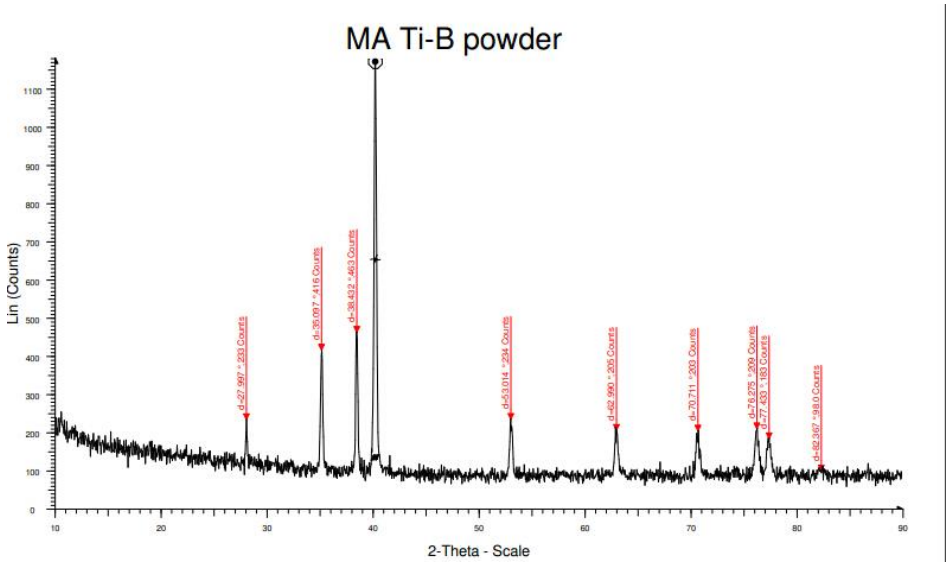

Figure 4.6 – XRD pattern of Ti-B powders ball-milled for 2h

4.5.2 Verification experiments of the Ti:B=1:2 model

When the molar ratio between titanium and boron is 1:2, Equation (8) can be rewritten as:

$$\frac{E_{system}}{n} = \int_{T_o}^{T_R} \left[c_p(T_i) + 2c_p(B)\right] dT + \int_{T_R}^{T_F} c_p(T_iB_2)\, dT + L_l(T_iB_2) + L_v(T_iB_2) \qquad (22)$$

This is a general equation with the assumption that the energy input on the left hand side is high enough to trigger all the changes on the right hand side. However, sometimes the changes on the right hand side may only partially happen. To better understand it, several intervals are created based on energies.

$E_1 = \int_{T_o}^{T_R} \left[c_p(T_i) + 2c_p(B)\right] dT$=20.08 kJ/mol: Energy required to trigger the reaction.

$E_2 = \int_{T_o}^{T_R}\left[c_p(T_i) + 2c_p(B)\right]dT + \int_{T_R}^{T_M(T_iB_2)} c_p(T_iB_2)\,d$=145.85 kJ/mol : Energy required to raise the whole system to the melting temperature of TiB_2, without melting.

$E_3 = \int_{T_o}^{T_R}\left[c_p(T_i) + 2c_p(B)\right]dT + \int_{T_R}^{T_M(T_iB_2)} c_p(T_iB_2)\,dT + L_l(T_iB_2)$ =246.25 kJ/mol: Energy required to melt TiB_2.

Since there is no enough vaporization information of the compound of TiB_2, the vaporization energy cannot be calculated.

The molar ratio is 1:x=1:2:

$$n = n_{T_i} = \frac{\pi d^2 h \rho_{T_i} \rho_B (1-\varepsilon)}{4\left(\rho_B M_{T_i} + 2\rho_{T_i} M_B\right)} = 5.5 \times 10^{-9}\ \text{mol} \quad (23)$$

The laser parameters of this experiment are: laser power 30 W; scanning speed 7 m/s. This energy input triggered the reaction of titanium and boron, and the reaction spread to the surrounding area where a dramatic burning phenomenon is observed.

Based on the laser parameter,

$$\frac{E_{laser\_absorption}}{n} = \frac{APd/v}{n} = 27.27\ \text{kJ/mol} > 20.08\ \text{kJ/mol} = E_1$$

This means that the absorbed laser energy can trigger the reaction between titanium and boron which is the case of the experiment. For the surrounding area where there is no laser energy input:

$$\frac{E_{reaction\_absorption}}{n} = A'|\Delta G(T_iB_2)| = 30\ \text{kJ/mol} > 20.08\ \text{kJ/mol} = E_1$$

The absorbed reaction energy can continue triggering the reaction, which means that the titanium and boron reaction is self-sustainable of this molar ratio under this certain condition. This is in good agreement with the burning phenomenon of the experiment.

For the area where there was laser energy input and also the energy obtained from the reaction.

$$\frac{E_{system}}{n} = \frac{E_{laser\_absorption} + E_{reaction\_absorption}}{n} = 57.27\frac{kJ}{mol} < 145.85\ \frac{kJ}{mol} = E_2$$

This indicates that the energy of the laser irradiation zone cannot melt the newly generated TiB_2.

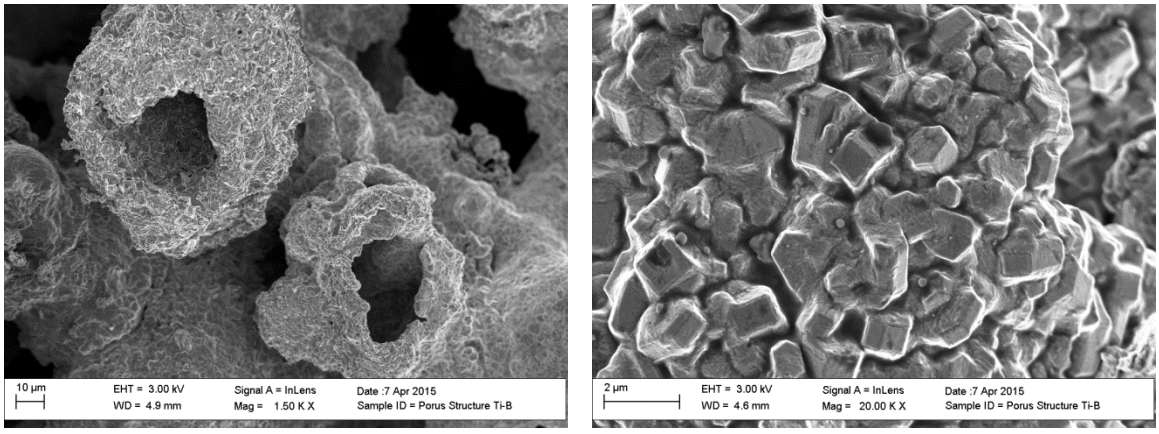

(a) **(b)**

Figure 4.7 – SEM images of the laser irradiation zone (a) porous structure (b) TiB_2

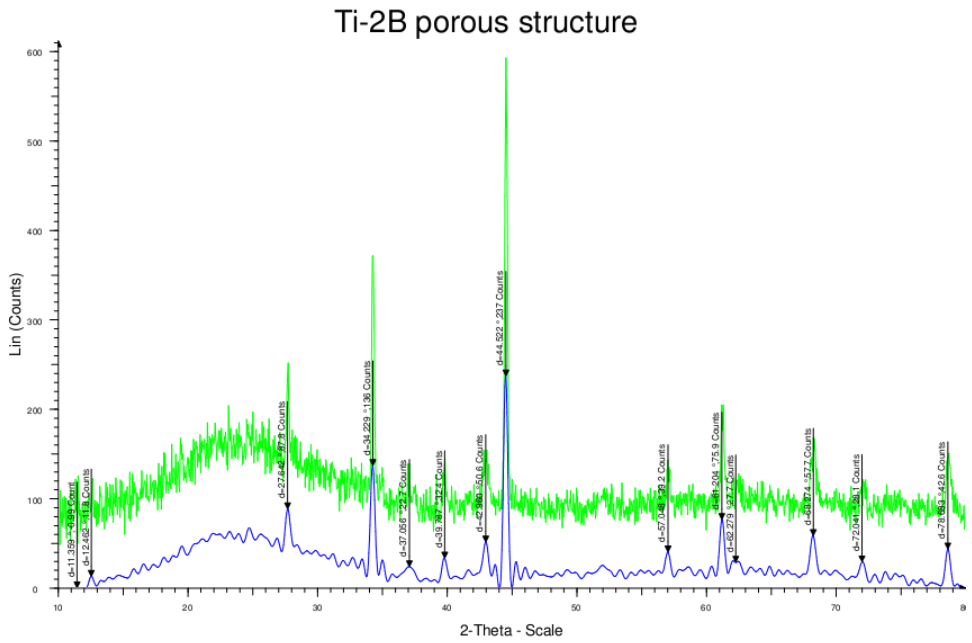

Figure 4.8 – XRD pattern of the TiB_2 porous structure zone

Figure 4.8 shows the XRD pattern of the porous structure zone, which proved the formation of TiB_2. And the microstructure of the newly formed TiB_2 can be observed in Figure 4.7b. The porous structure is shown in Figure 4.7a. The pores are in spherical shape with an average diameter of 20 μm which is in the same order of magnitudes of titanium (spherical, 15～45μm). So, it can be concluded that the spherical pores are where the initial titanium powders locate. Since the energy input of the irradiation zone is not high enough to melt TiB_2, the randomly distributed TiB_2 bulks could not collapse or flowed into a solid and dense part.

To at least melt T_iB_2, high energy input by defining the test series was carried out. The laser power and scanning speed are two controlled parameters as is shown in Figure 4.9. From the left to the right column, the values of laser power increase from 144 to 198 W. From the top to the bottom row, the values of scanning speed decrease from 708 to 531 mm/s. So it can be concluded that laser energy inputs increase from the left top corner to the right bottom corner. The black squares inside each cavity are the laser irradiation zones.

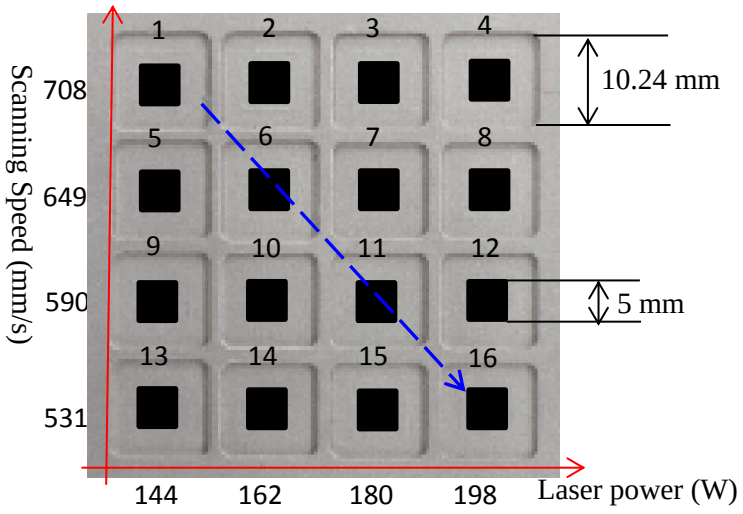

Figure 4.9 – Test series on the loose powder

The calculated E_{system}/n values are between 1324.30 kJ/mol and 2402.88 kJ/mol. These values are extremely higher than the energy required (246.25 kJ/mol) to melt TiB_2. However, the laser absorption coefficient of TiB_2 is different from that of the mixture of titanium and boron. And the molar heat capacity of TiB_2 at elevated temperature is different than that of TiB_2 at low temperature. All these factors make it hard to get the exact value of energy to evaporate TiB_2.

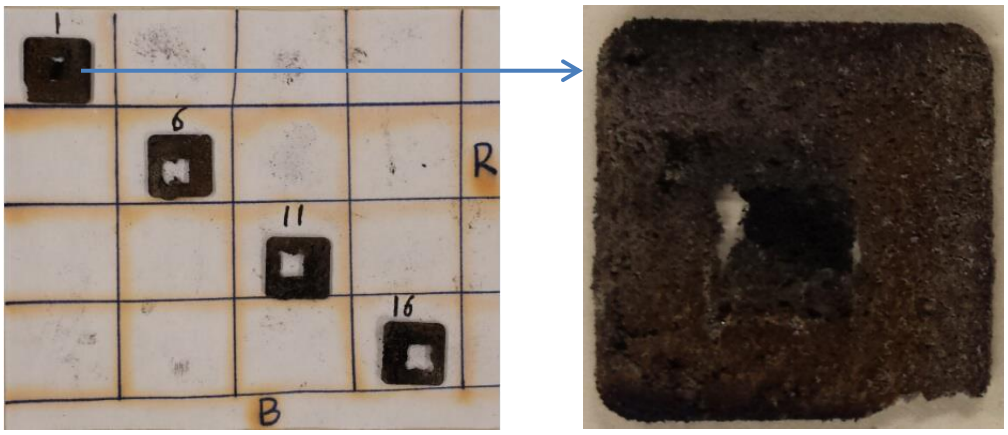

(a)

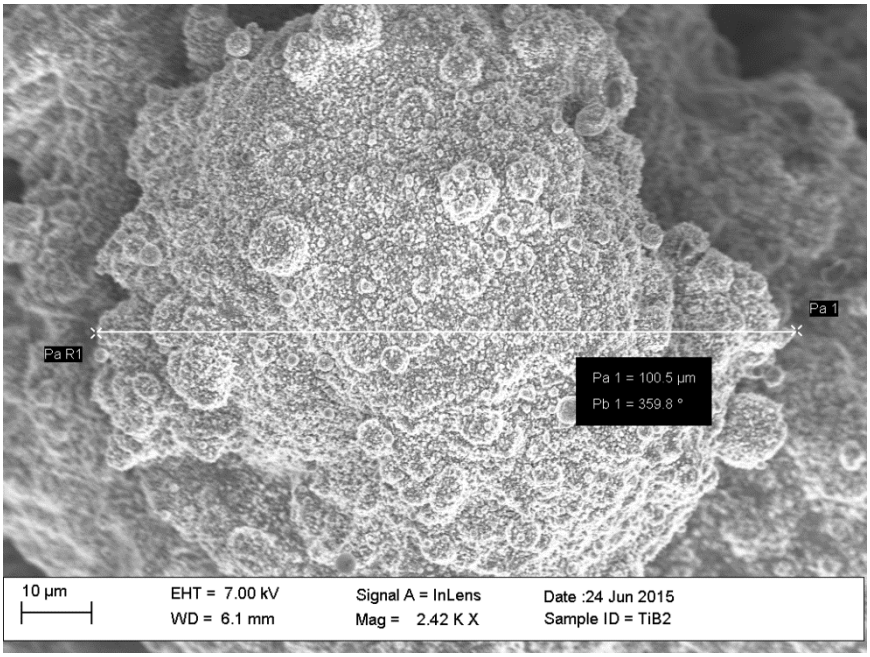

(b)

Figure 4.10 – (a) Test series results of the printed parts of sample 1, 6, 11, and 16; (b) SEM image of the center area of sample 1

Figure 4.10a shows the experiment results of the test series. The hollow areas in the center (laser irradiation zone) of sample 6, 11, and 16 indicate the vaporization of TiB_2. For sample 1, there is still material in the center of the irradiation zone. As analyzed above, even the lowest energy input can melt the newly formed TiB_2. This is the reason why the height of the center square of sample 1 is lower than that of the surrounding area. The big chunk with the size of 100.5 µm shown in Figure 4.10b indicates the melt of the formed TiB_2. Compare to the microstructure of Figure 4.7a, there is no obvious hollow structure of Figure 4.10b which is also a proof that melt occurred with the high laser energy input.

4.5.3 Verification experiments of the Ti:B=4:1 model

If the molar ratio between titanium and boron is 4:1 $(1: 1/4)$, Equation (10) can be rewritten as:

$$\frac{E_{system}}{n} = \frac{1}{4}\int_{T_o}^{T_R} c_p(B)\,dT + \int_{T_o}^{T_R} c_p(T_i)\,dT + \frac{3}{4}\left[\int_{T_R}^{T_F} c_p(T_i)dT + L_l(T_i) + L_v(T_i)\right] + \frac{1}{4}\left[\int_{T_R}^{T_F} c_p(T_iB)\,dT + L_l(T_iB) + L_v(T_iB)\right] \quad (24)$$

Similar to the model of T_i:B=1:2, several intervals are created based on energy requirements:

$E_1 = \frac{1}{4}\int_{T_o}^{T_R} c_p(B)\,dT + \int_{T_o}^{T_R} c_p(T_i)\,dT$ =11.91 kJ/mol: Energy required to trigger the reaction.

$E_2 = \frac{1}{4}\int_{T_o}^{T_R} c_p(B)\,dT + \int_{T_o}^{T_R} c_p(T_i)\,dT + \frac{3}{4}\int_{T_R}^{T_M(T_i)} c_p(T_i)dT + \frac{1}{4}\int_{T_R}^{T_M(T_i)} c_p(T_iB)\,dT$ =

50.33 kJ/mol: Energy required to raise the whole system to the melting temperature of Ti, without melting.

$$E_3 = \frac{1}{4}\int_{T_o}^{T_R} c_p(B)\,dT + \int_{T_o}^{T_R} c_p(T_i)\,dT + \frac{3}{4}\left[\int_{T_R}^{T_M(T_i)} c_p(T_i)dT + L_l(T_i)\right] + \frac{1}{4}\int_{T_R}^{T_M(T_i)} c_p(T_iB)\,dT$$

=60.94 kJ/mol: Energy required to raise the whole system to the melting temperature of Ti, with the melting of Ti.

$E_4 =$

$$\frac{1}{4}\int_{T_o}^{T_R} c_p(B)\,dT + \int_{T_o}^{T_R} c_p(T_i)\,dT + \frac{3}{4}\left[\int_{T_R}^{T_M(T_iB)} c_p(T_i)dT + L_l(T_i)\right] + \frac{1}{4}\int_{T_R}^{T_M(T_iB)} c_p(T_iB)\,dT$$

=77.73 kJ/mol: Energy required to raise the whole system to the melting temperature of TiB, without the melting of TiB.

The molar ratio is 1:x=4:1, then:

$$n = n_{T_i} = \frac{\pi d^2 h \rho_{T_i} \rho_B (1-\varepsilon)}{4\left(\rho_B M_{T_i} + \frac{1}{4}\rho_{T_i} M_B\right)} = 9.7 \times 10^{-9}\ \text{mol} \tag{25}$$

This section is arranged as follows: First, lines printed by laser were analyzed; Second, parameters that could create one flat surface were optimized; Third, the optimized parameters were used to print multiple layers (parts).

4.5.3.1 Reaction assisted alloy process

A test series of 4×4 samples with laser powder from 80 W to 170 W, and scanning speed from 3 m/s to 0.9 m/s on the solid substrate was designed to investigate the effect of reaction on the alloy process.

Based on the laser parameter,

$$\frac{E_{laser\_absorption}}{n} = \frac{APd/v}{n} = 96.22 \sim 681.56\ \text{kJ/mol} > 11.91\ \text{kJ/mol} = E_1$$

This means that the absorbed laser energy can trigger the reaction between titanium and boron. For the surrounding area where there was no laser energy input:

$$\frac{E_{reaction\_absorption}}{n} = A'\left|\frac{1}{4}\Delta G(T_iB)\right| = 4\ \text{kJ/mol} < 11.91\ \text{kJ/mol} = E_1$$

This indicates that the titanium and boron reaction of the molar ratio of 4:1 under this condition is not self-sustainable. For the laser irradiation zone:

$$\frac{E_{system}}{n} = \frac{E_{laser\_absorption} + E_{reaction\_absorption}}{n} = 100.22\sim685.56\ kJ/mol > E_3$$

According to the above, the energy input of the combination of laser irradiation and reaction can totally melt the residual T_i.

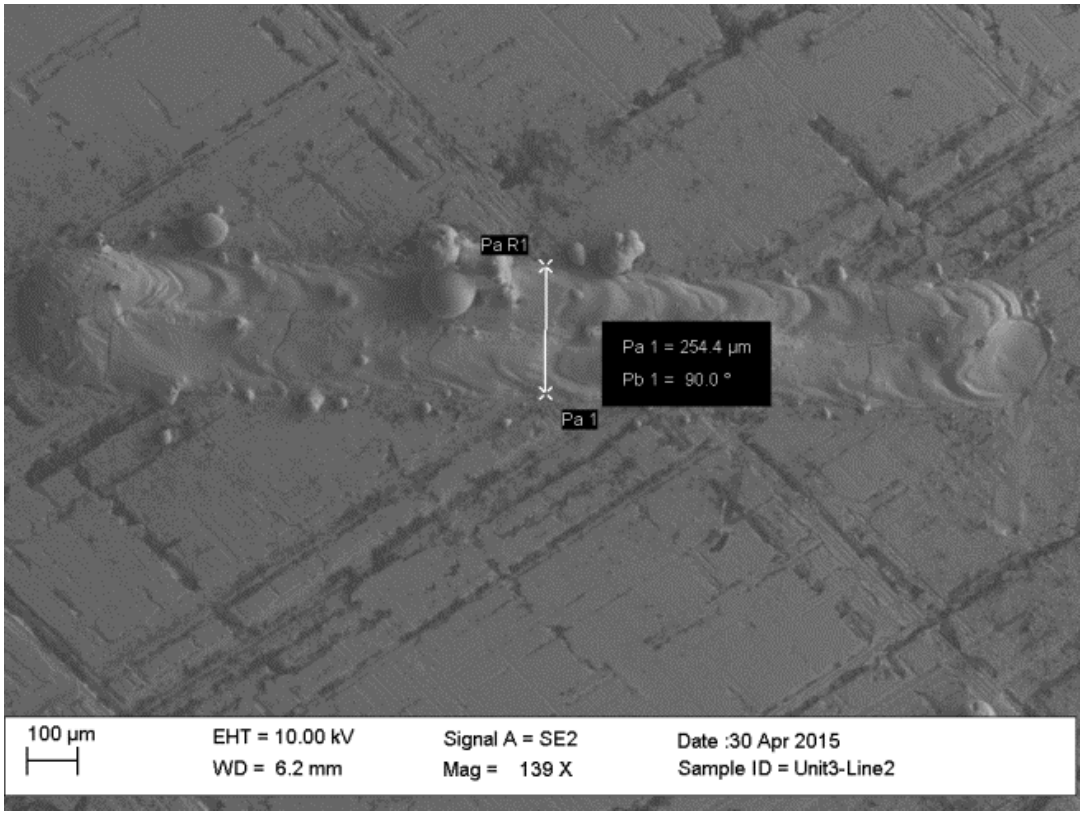

(a)

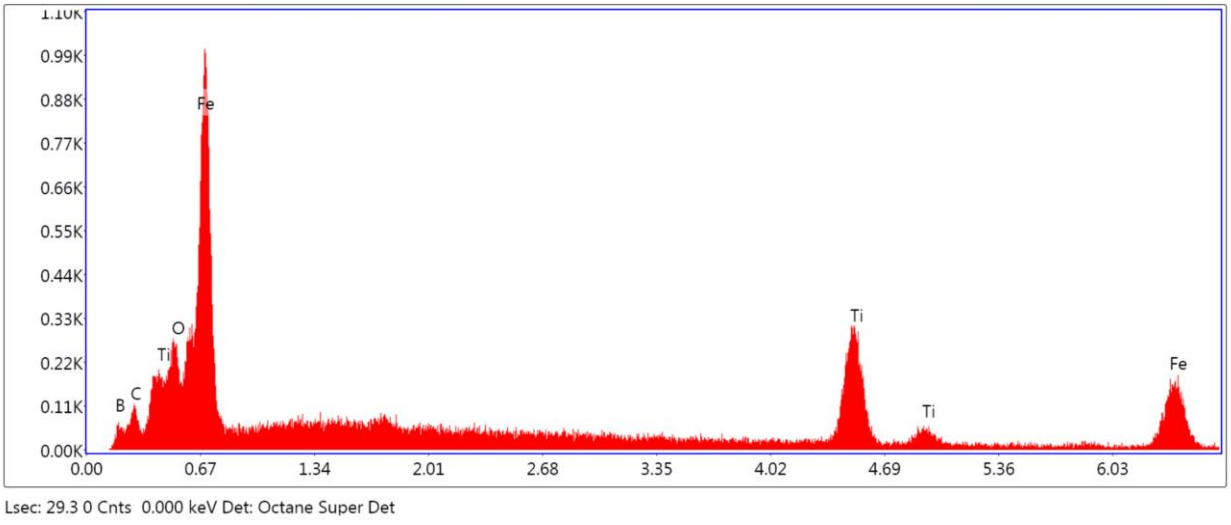

(b)

Figure 4.11 – Sample 3 of the test series (a) SEM image, (b) Energy-dispersive X-ray spectroscopy (EDAX) elemental analysis

The designed width of the line is 200 μm, while the real width of the line is 25% wider (254.4 μm) as is shown in Figure 4.11a. High laser energy input (168.39 kJ/mol) combining with the energy obtained from the reaction contribute to this phenomenon. Since the hatch distance of the laser is 100μm, the laser needs to scan twice to finish the designed line. This is confirmed by the two tracks with opposite arcs. Part of the energy is conducted to the surrounding area and also to the substrate, causing the reactions and melting of the surrounding area and the substrate. The existence of iron and carbon as is show in Figure 4.11b proves the melting of substrate (the substrate is made of stainless steel for this experiment). The melting of the powder system due to the high energy input created a relatively flat surface, especially the middle of the line. Because the air in the chamber cannot be totally vacuumized of the AM250 machine, there was still oxygen left with argon. So the processing of the powder was poisoned with the appearance of oxygen (Figure 4.11b). The spherical particles shown in Figure 4.11a are titanium particles from the surrounding area.

4.5.3.2 Fine surface creation by optimizing laser parameters

A test series of 4×4 samples with laser powder from 30 W to 120 W, and scanning speed from 5 m/s to 2 m/s on the ceramics was designed. The differences between this experiment and the experiment form Section 4.5.3.1 lie in the substrate and shape of the samples. Ceramics substrate was used to avoid the affection of stainless steel. The affection of stainless steel is extremely high especially when only one or just a few layers are printed. The square samples

were printed instead of line samples. Since ceramics has a lower heat conductivity than that of stainless steel, lower laser power were adopted for this experiment.

The energies for each sample, calculated based on the models created before, are shown in Table 4.3. When the laser power was 30 W, the energies generated could not fully melt the residual Ti (energy required is 60.94 kJ/mol) regardless of the scanning speeds arranging from 5 m/s to 2 m/s. Due to the short of the value of TiB's latent heat of liquefaction, the energy required to fully melt TiB is unknown. However, this energy value should be at least greater than E_4 =77.73 kJ/mol, the energy required to raise the whole system to the melting temperature of TiB. Based on the experiment results, the solid complete surface layers can be obtained with the laser power of 120 W, despite of the scanning speed. Thus, it can be concluded that the energy required to fully melt the whole system is between 77.73 kJ/mol and 90.60 kJ/mol. The red-highlighted values in Table 4.3 are the values that satisfy this requirement. And the related sample numbers of these values are: 4, 8, 11, 12, 14, 15, and 16. Figure 4.12 shows that the surface of sample 4, 8, 12, 15, and 16 were relatively complete and attached well to the ceramics substrate which are in good agreement with the energies values calculated in Table 4.3. If the energy values are not high enough to fully melt the powder layer, the printed powder layer will be brittle and cannot even connect well with the surrounding materials, which is the case for the rest of the samples.

If the energy required to fully melt the newly formed TiB (E_5) is 90.60 kJ/mol, then:

$$\frac{1}{4}\mathrm{L_l(T_iB)} = \mathrm{E_5} - \mathrm{E_4} = 12.87\ \mathrm{kJ/mol}$$

So the latent heat of liquefaction of TiB is 51.48 kJ/mol. However, since 90.60 kJ/mol is not the critical value to melt the TiB, the latent heat of liquefaction of TiB should be less than or

equal to 51.48 kJ/mol. Compare to the latent heat of liquefaction of Ti $L_l(T_i) = 14.15$ kJ/mol, B $L_l(B) = 50.2$ kJ/mol, and TiB_2 $L_l(T_iB_2) = 100.4$ kJ/mol, this value is reasonable.

Table 4.3 – Energy matrix of the test series

Laser power (W) / Scanning speed (m/s) — Energy (kJ/mol)	30	60	90	120
5	25.65	47.30	68.95	90.60
4	31.06	58.12	85.18	112.25
3	40.08	76.16	112.25	148.33
2	58.12	112.25	166.37	220.49

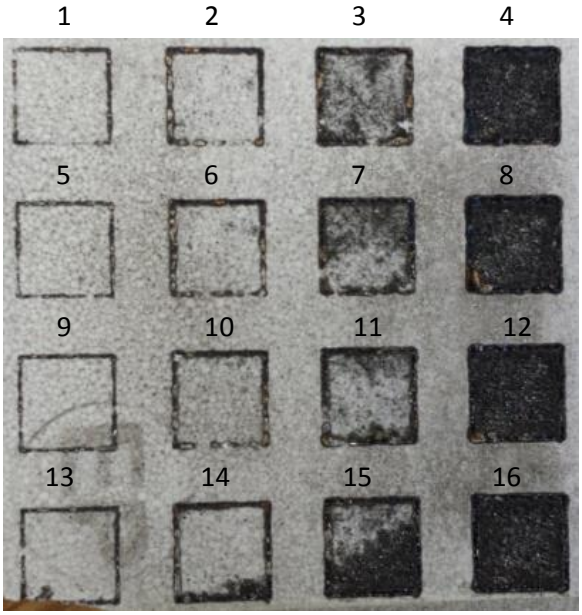

Figure 4.12 – Experiment results of the test series

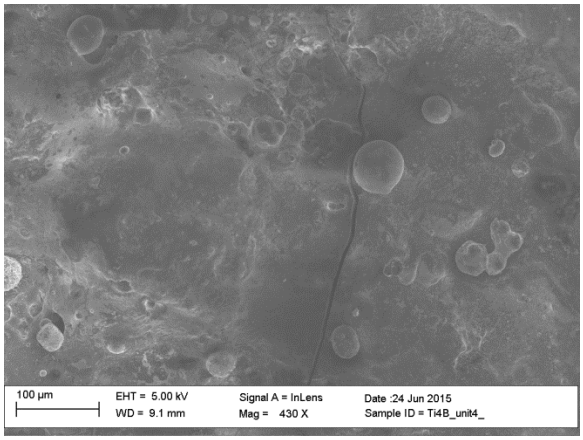
100 µm
EHT = 5.00 kV
WD = 9.1 mm
Signal A = InLens
Mag = 430 X
Date :24 Jun 2015
Sample ID = Ti4B_unit4_

(a)

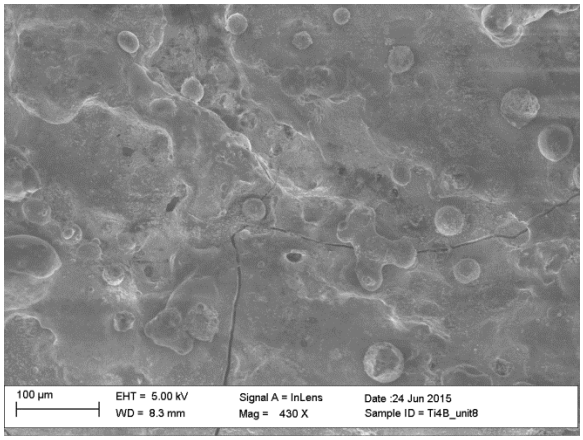
100 µm
EHT = 5.00 kV
WD = 8.3 mm
Signal A = InLens
Mag = 430 X
Date :24 Jun 2015
Sample ID = Ti4B_unit8

(b)

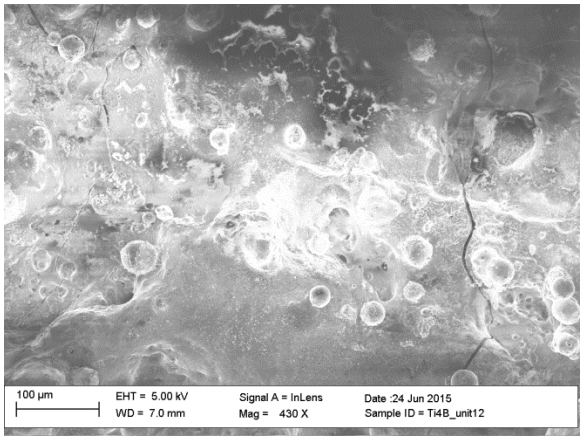
100 µm
EHT = 5.00 kV
WD = 7.0 mm
Signal A = InLens
Mag = 430 X
Date :24 Jun 2015
Sample ID = Ti4B_unit12

(c)

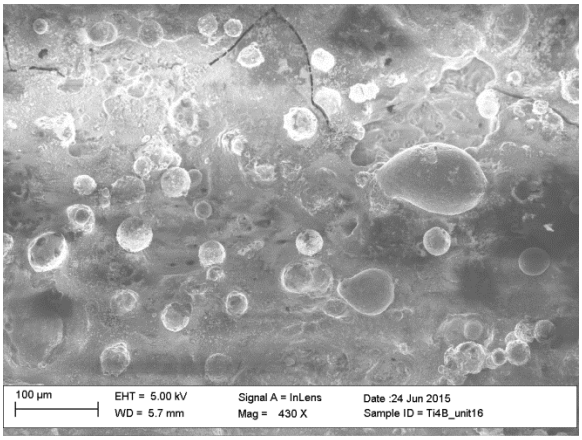
100 µm
EHT = 5.00 kV
WD = 5.7 mm
Signal A = InLens
Mag = 430 X
Date :24 Jun 2015
Sample ID = Ti4B_unit16

(d)

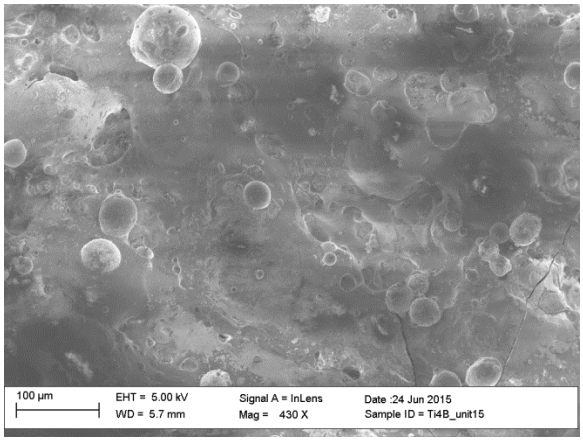
100 µm
EHT = 5.00 kV
WD = 5.7 mm
Signal A = InLens
Mag = 430 X
Date :24 Jun 2015
Sample ID = Ti4B_unit15

(e)

Figure 4.13 – SEM images of the laser processed surfaces of sample (a) 4 (b) 8 (c) 12 (d) 16 and (e) 15 with the magnification of 430 ×

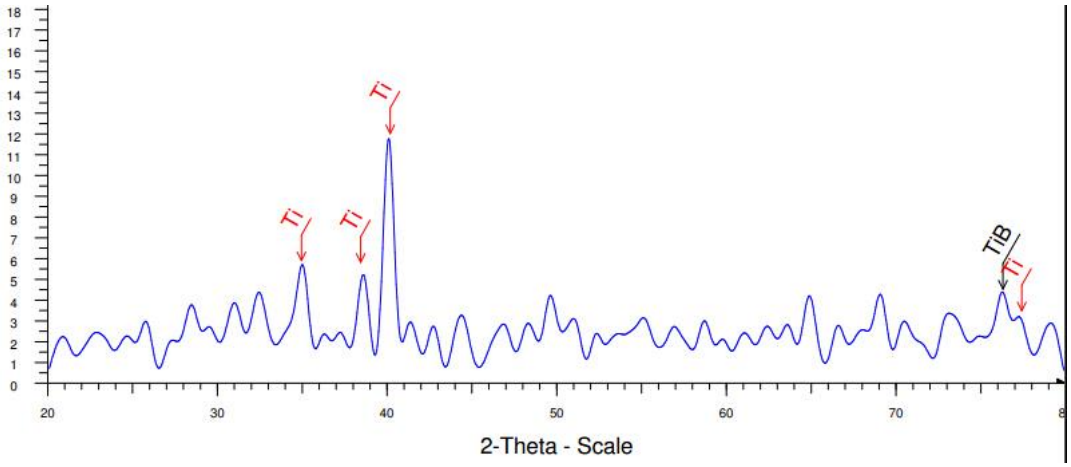

Figure 4.14 XRD pattern of sample 12

SEM images of the microstructures of sample 4, 8, 12, 16, and 15 are shown in Figure 4.13 with the same magnification of 430 ×. It can be seen that the surfaces are smooth without obvious wrinkles. This indicates that the laser processing parameters are good enough to create high quality of surface finish. However, the appearance of cracks, caused by rapid and uneven cooling and unbalance distribution of the titanium and boron powder of the irradiated area, is a significant defect of building metallic layers on the ceramics substrate. The heat conductivity of ceramics differs a lot from that of metallic material which is the main reason of the uneven cooling. Since the scanning speed is as fast as 2∼5 m/s, some of the titanium particles with large size cannot be fully melted or react with the surrounding boron powder. Thus, titanium particles can still be seen in Figure 4.13. According to the analysis, laser power of 120 W is better than any other laser energy inputs of this experiment. In addition, TiB is detected with the scanning speed of 3 m/s under this laser energy input (Figure 4.14). Therefore, the laser power parameter of 120 W is selected as the initial setting for the following experiment to build multiple layers with smooth surfaces.

4.5.3.3 Build of multiple layers with proper parameters

The parameters for the build of multiple layers are listed in Table 4.4. The red-highlighted column shows the initial setting, obtained from Section 4.5.3.2, of the laser processing. Due to the limitation of the machine, the powders were manually spread instead of spreading by the wiper mounted inside the chamber of the AM250 machine which resulted in the unequal powder distribution within one layer and different layer thicknesses between multiple layers. These problems can give rise to the uneven surface finish and cracks between two layers. Figure 4.15a illustrates the rough surfaces of the printed parts except sample 4 and sample 16. Thus, it can be assumed that solid parts with good surface morphology can be obtained under these laser parameters with proper way of spreading powder. On account of unequal and improper layer thicknesses between different layers, the cracks and gaps between different layers, circled by red-dash lines, are observed in Figure 4.15b.

Table 4.4 – Parameters of building multiple layers

Laser power (W) / Scanning speed (m/s)	80	100	120	140
5	Sample 1	Sample 2	Sample 3	Sample 4
4	Sample 5	Sample 6	Sample 7	Sample 8
3	Sample 9	Sample 10	Sample 11	Sample 12
2	Sample 13	Sample 14	Sample 15	Sample 16

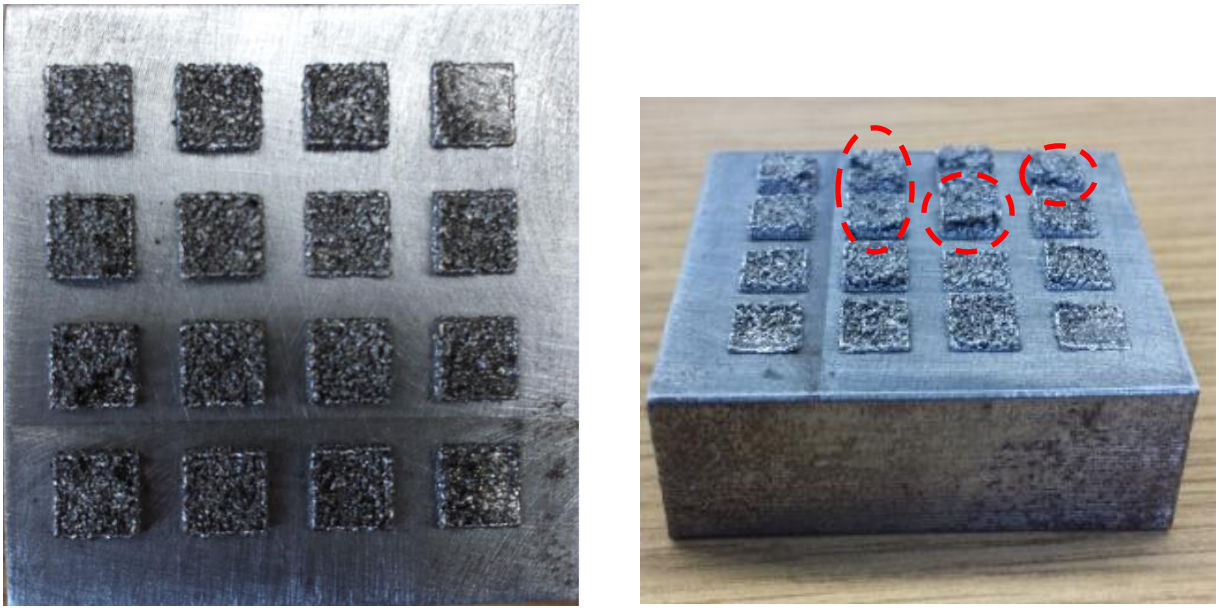

(a) **(b)**

Figure 4.15 – (a) Top view, and (b) side view of the printed parts with multiple layers

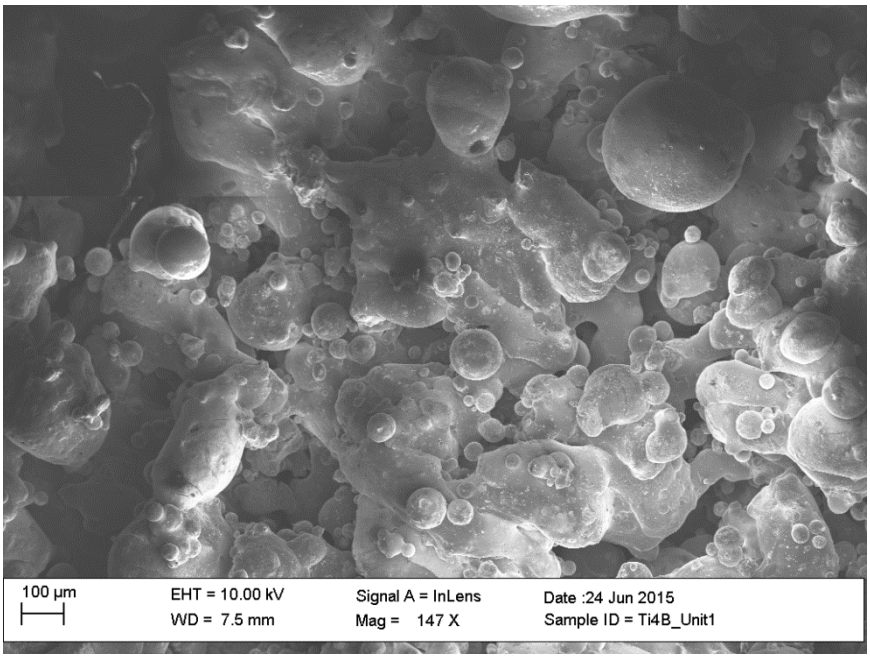

(a)

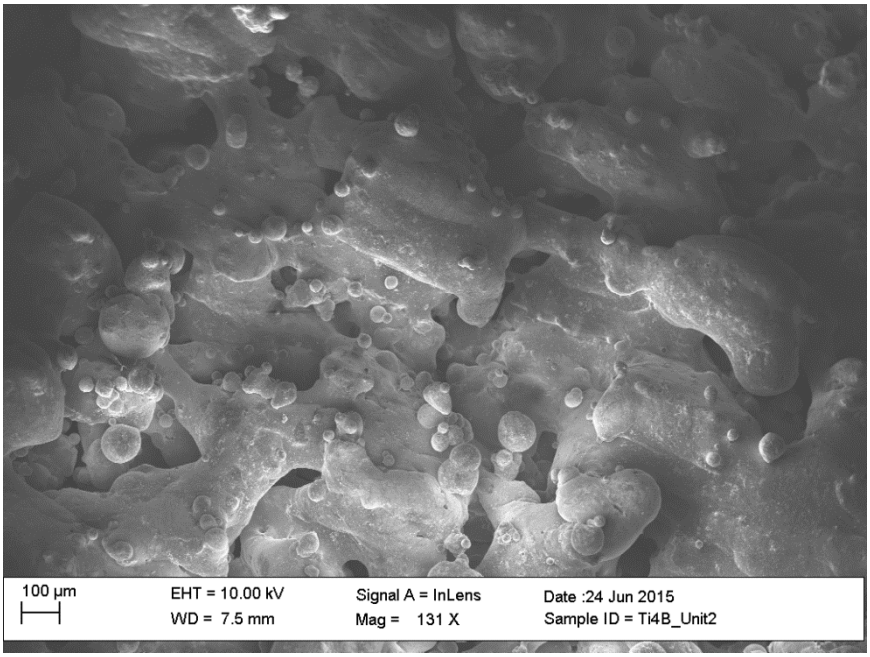
100 µm
EHT = 10.00 kV
WD = 7.5 mm
Signal A = InLens
Mag = 131 X
Date :24 Jun 2015
Sample ID = Ti4B_Unit2

(b)

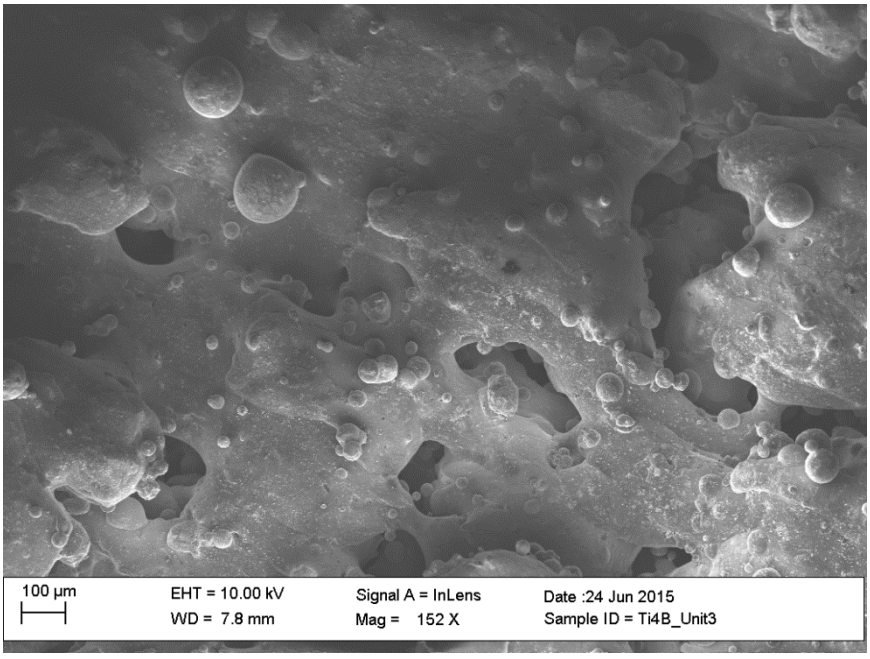
100 µm
EHT = 10.00 kV
WD = 7.8 mm
Signal A = InLens
Mag = 152 X
Date :24 Jun 2015
Sample ID = Ti4B_Unit3

(c)

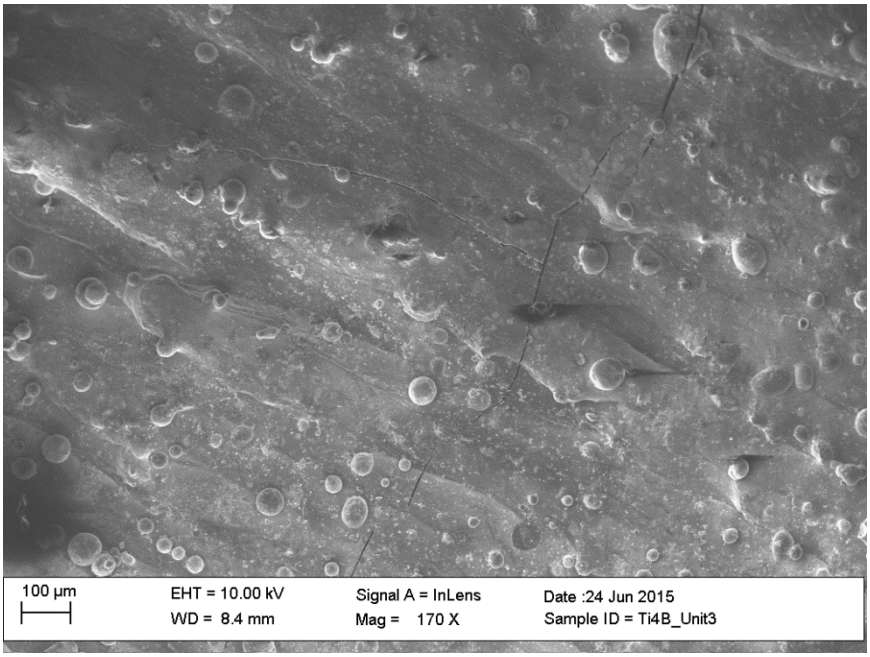

(d)

Figure 4.16 SEM images of surface morphology of sample 1, 2, 3, and 4

To have a better view of the surface morphology, SEM images of top surface of sample 1, 2, 3, and 4 were taken. Figure 4.16a shows the microstructure of the top surface of sample 1. Big gaps between different melted chunks indicate that parameters of sample 1 can only partially melt the powder system with pores inside the solid. At the same time, there is still a great amount of titanium particles left. As for sample 2 (Figure 4.16b), the average sizes of the chunks are bigger than that of sample 1 with relatively flat surface. The increasing of laser energy reduces the number of not-melted and unreacted titanium powders as well. When increasing the laser energy from 100 W to 120 W, the printed part is almost fully melted with small and few pores inside which can be seen in Figure 4.16c. However, the defects of the existing of pores and titanium particles cannot be avoided. Figure 4.16d shows the surface morphology of sample 4 with the highest laser energy of 140 W. It can be noted that there are no pores or big gaps of the top surface. So the laser energy of 140 W is the optimal parameter when the laser scanning speed

is 5 m/s. Nevertheless, titanium particles still exist regardless the energy inputs under this scanning speed condition.

CHAPTER V

CONCLUSION AND DISCUSION

5.1 Overview of this Chapter

This chapter summarizes the findings and conclusions of this thesis work. At the same time, the limitations and shortcomings occurred during the theoretic models creation and multiple layers building process are pointed out. As for these problems, further work that needs to be done in the future is discussed.

5.2 Findings and Conclusions of this Thesis

The main purpose of this thesis is to understand the selective laser alloying process of elemental titanium and boron powder. One of the challenges is that titanium and boron may react with each other and release a huge amount of energy during the laser processing. The reactions and energy released make the alloying process hard to control and analyze. To better understand the alloying process, theoretic models of the selective laser alloying process of the mixture of elemental titanium and boron powder were created.

Since different compounds with different reactions can be formed between titanium and boron, three models were developed based on the molar ratio between these two elements. The three general models take the related chemical and physical phenomena into account, such as

the reaction between titanium and boron, the liquefaction (fusion) and vaporization of titanium, boron and their alloy. On account of different energy input and energy absorbed, all or part of the phenomena can be expected. The first model is when the molar ratio between titanium and boron is less than 1:2. TiB_2 is the only compound formed under this circumstance. The second model assumes the over dose of titanium with the formation of TiB only. When the molar ratio of titanium and boron is between 1:2 and 1:1, the formation of compounds TiB_2, TiB, Ti_3B_4 perplexes the problem and introduces more uncontrollable factors. Thus, the third model is not the focus of this thesis.

After the development of the theoretic models, the values of the corresponding variables were settled based on references and information provided by the related machines. However, some of the variable values were missing due to the lack of data and some of them were treated as constants despite that these properties are temperature-dependent to simplify the problem.

The designing of test series was utilized to test a number of samples with different parameters of laser power and scanning speed at the same time. Not only processing time, but also materials are saved by the test series strategy. To achieve different goals, two types of melting mechanisms were investigated: melting on the solid substrates of stainless steel or ceramics; melting on the loose powder substrate of aluminum. The purpose of the replacement of stainless steel substrate to ceramics substrate was to eliminate the effect of elemental iron and carbon on the testing materials.

To avoid the pre-alloy phenomenon, appropriate mixture of parameters have been selected for the ball-mill procedure. Taking the uniform distribution and small shallow cavities among the boron matrix into consideration, 2 h ball-milling was the optimal milling time for the

preparation of the mixture of titanium and boron of the follow-up process. The XRD analysis demonstrated that no compounds were created and only elemental titanium and boron were detected.

After all the preliminary work, the experiments with molar ratios of 1:2 and 4:1 between titanium and boron were carried out and analyzed, respectively.

For the molar ratio of 1:2, the reaction was triggered with the parameters: laser power 30 W; scanning speed 7 m/s. Since the reaction was self-sustainable as calculated, burning phenomenon of the irradiation zone and also the surrounding area was observed. The SEM images of the irradiation zone indicated the formation of TiB_2 and also porous structure. This experiment was categorized as low energy input experiment on account of the not-melted TiB_2. To raise the energy input, new parameters were assigned to the samples of test series: laser power 144~198 W; scanning speed 708~531 m/s. The energy absorbed by the powder system was so high that evaporation occurred to sample 6, 11, and 16 with nothing left at the laser irradiation zone. For the reason that the energy input of sample 1 was relatively lower than any other samples, only part of the material at the laser irradiation zone evaporated. This experiment is categorized as high energy input. It can be seen that all the experiments under this certain molar ratio are in good agreement with the theoretic model developed before. And the model did help for the analysis of the experiment results.

When the molar ratio is 4:1, three different experiments were conducted in the order of line→ surface→ part. First, lines were printed, the parameters of which provided reference for the surface printing process. However, taking the low heat conductivity of ceramics substrate into consideration, the energy range designed for the surface printing is lower than that of line

printing. Smooth surfaces without obvious wrinkles or any other defects were obtained under some certain conditions. And it is proved that high quality of surface finish was achieved with the laser power of 120 W, despite the scanning speed parameter. Thus, for the building of solid parts (multiple layers), the laser power of 120 W was chosen as the initial setting. Because of the limitation of the machine, the mixture powder was manually spread on the substrate, which gave rise to the uneven powder distribution within one layer and uncontrollable layer thicknesses of different layers. These flaws leaded to the rough surface finish and cracks between two layers as was observed of the experiment results. With the increasing of laser power, the defects such as partially melt of the powder system with pores inside the solid part and uneven surface could be weakened or eliminated. Therefore, the laser power of 140 W was the optimal parameter under which solid parts and flat surface were created. Under this laser power condition, the parameter of scanning speed had small effect on the alloying process.

In addition, the estimation of the latent heat of liquefaction of TiB based on the theoretical model and experiment result provides a way of figuring out missing data.

5.3 Future Work

Although to some degree, the theoretic models are in good agreement with the experiment results and help understand the selective laser alloying process of elemental titanium and boron powder system, there are still some limitations and shortcomings of the models and the printing process. These problems which need more future work are pointed out as follows:

- Due to the complex process of selective laser alloying of the titanium and boron powder system and shortage of related experiment facilities, some of the affecting factors are missing, such as the dissipation coefficient of energy during the reaction,

the latent heat of vaporization of the formed compounds. Some of the affecting factors are temperature-dependent, such as molar heat capacity and density, which cannot be treated as constant values. The existence of oxygen is unavoidable and affects the analysis of the experiment results via reacting with titanium powder. Thus, more work needs to be done on the unknown variable values, and the poison oxygen should be controlled at an even lower level.

- To simplify the theoretic model creation, a "top hat" laser beam with identically distributed laser powder is adopted instead of Gaussian-distributed laser power. In reality, rather than a cylinder volumetric heating area, the melting pool under the Gaussian-distributed laser power exhibits a semi-spherical shape. Therefore, a Gaussian-distributed laser power with the consideration of heat transfer should be modeled in the future work.
- When taking the unknown variable values and complicated reaction situation into account, the molar ratio of titanium and boron between 1:2 and 1:1 is not studied by this thesis which can be future work.
- When printing multiple layers, manually spreading of powder makes the top surfaces of solid parts rough and cracks exist between two adjacent layers. In the future, new dosing mechanism which can overcome these problems needs to be designed and carried out.

REFERENCES

1. Atri, R.R., Ravichandran, K.S., & Jha, S.K. (1999). Elastic properties of in-situ processed Ti-TiB composites measured by impulse excitation of vibration. Materials Science and Engineering. A 271 (1), 150-159.

2. Attar, H., Bönisch, M., Calin, M., Zhang, L.C., Scudino, S., & Eckert, J. (2014). Selective laser melting of in situ titanium-titanium boride composites: processing, microstructure and mechanical properties. Acta Materialia. 76, 13-22.

3. Barin, I. (1995). Thermochemical Data of Pure Substances. Third ed, VCH, Weinheim.

4. Bermingham, M.J., McDonald, S.D., Nogita, K., John, D.H.St., & Dargusch, M.S. (2008). Effect of boron on microstructure in cast titanium alloys. Scripta Materialia. 59, 538-541.

5. Boron. In Wikipedia. Retrieved June 21, 2015, from https://en.wikipedia.org/wiki/Boron

6. Brondin, H., Andersson, O., & Johansson, S. (2013). Mechanical testing of a selective laser melted superalloy. 13th International Conference on Fracture.

7. Campanelli, S.L., Contuzzi, N., Angelastro, A., & Ludovico, A.D. (2010) Capabilities and performances of the selective laser melting process. New Trends in Technologies: Devices, Computer, Communication and Industrial Systems, Meng Joo Er (Ed.), ISBN: 978-953-307-212-8, InTech, DOI: 10.5772/10432. Available from: http://www.intechopen.com/books/new-trends-in-technologies--devices--computer--communication-and-industrial-systems/capabilities-and-performances-of-the-selective-laser-melting-process.

8. Campanelli, S.L., Contuzzi, N., Anglastro, A., & Ludovico, A.D. (2010). Capabilities and performances of the selective laser melting process. INTECH Open Access Publisher.

9. Carslaw, H.S., & Jaeger, J.C. (1959). Conduction of heat in solids. Oxford University Press, Amen House, London E.C.4.

10. Chandrasekar, P., Balusamy, V., Ravi Chandran, K.S., & Kumar, H. (2007). Laser surface hardening of titanium-titanium boride (Ti-TiB) metal matrix composite. Scripta Materialia. 56, 641-644.

11. Chase, M.W., Jr. (1998). NIST-JANAF Themochemical Tables, Fourth Edition. Journal of Physical and Chemical Reference Data, Monograph 9.

12. Conventional Atomic Weights. (2013). Commission on Isotopic Abundances and Atomic Weights.

13. Feng, H., Meng, Q., Zhou, Y., & Jia, D. (2005). Spark plasma sintering of functionally graded material in the Ti-TiB2-B system. Materials Science and Engineering A. 397(1-2), 92-97.

14. Gebhardt, A., Schmidt, F.M., Hötter, J.S., Sokalla, W., & Sokalla, P. (2010). Additive manufacturing by selective laser melting the realizer desktop machine and its application for the dental industry. Physics Procedia, 5, 543-549.

15. Gini, Andrea. (2012). Selective laser melting: the future of space manufacturing. Spacecraft Design. Retrieved March 25, 2015.

16. Gusarov, A.V., Yadroitsev, I., Bertrand, Ph., Smurov, I. (2009). Model of radiation and heat transfer in laser-powder interaction zone at selective laser melting. Journal of Heat Transfer. 131 (7), 072101.

17. Kaplan, A.F.H. (2011). Analysis and modeling of a high-power Yb:fiber laser beam profile. Optical Engineering. 50 (5), 054201.

18. Kartal, G., Timur, S., Urgen, M., & Erdemir, A. (2010). Electrochemical boriding of titanium for improved mechanical properties. Surface and Coatings Technology. 204(23), 3935-3939.

19. Kou, S., & Wang, Y.H. (1986). Three-dimensional convection in laser melted pools. Metallurgical and Materials Transactions A. 17A, 2265-2269.

20. Kruf, W., Van de Vorst, B., Maalderink, H., & Kamperman, N. (2006). Design for rapid manufacturing functional SLS parts. Proceeding of 5th CIRP Int. Conf. on Intelligent Computation in Manufacturing Engineering. 609-613.

21. Lide, D.R. (2009). CRC Handbook of Chemistry and Physics. 90th Edition. CRC Press (Taylor and Francis Group).

22. Li, Y., Yang, C., Zhao, H., Qu, S., Li, X., & Li, Y. (2014). New development of Ti-based alloys for biomedical applications. Materials. 7, 1709-1800.

23. Long, M., & Rack, H.J. (1998). A review: titanium alloys in total joint replacement-a materials science perspective. Biomaterials. 19, 1621-1639.

24. Makuch, N., Kulka, M., Dziarski, P., & Przestacki, D. (2014). Laser surface alloying of commercially pure titanium with boron and carbon. Optics and Laser in Engineering. 57, 64-81.

25. Matin, M.A., Lu, L., & Gupta, M. (2001). Investigation of the reactions between boron and titanium compounds with magnesium. Scripta Materialia. 45 (4), 479-486.

26. Mazumder, J., & Kar, A. (1995). Theory and application of laser chemical vapor deposition. Plenum Publishing Co., New York.

27. Mumtaz, K.A., Hopkinson, N., & Erasenthiran, P. (2008). High density selective laser melting of Waspaloy. Journal of Material Processing Technology, 195 (1), 77-87.

28. Panda, K.B., & Ravi Chandran, K.S. (2003). Titanium-titanium boride (Ti-TiB) functional graded materials through reaction sintering: synthesis, microstructure, and properties. Metallurgical and Materials Transactions A. 34A, 1371-1385.

29. Ravi Chandran, K.S., Panda, K.B., & Sahay, S.S. (2004). TiB_w-reinforced Ti composites: processing, properties, application prospects, and research needs. JOM. 56(5), 42-48.

30. Schmidt, J., Boehling, M., Burkhardt, U., & Grin, Y. (2007). Preparation of titanium diboride TiB2 by spark plasma sintering at slow heating rate. Science and Technology of Advanced Materials. 8, 376-382.

31. Shiomi, M., Yoshidome, A., Abe, F., & Osakada, K. (1999). Finite element analysis of melting and solidifying processes in laser rapid prototyping of metallic powders. International Journal of Machine Tools & Manufacture. 39, 237-252.

32. Standard Atomic Weights. (2013). Commision on Isotopic Abundances and Atomic Weights.

33. Tamirisakandala, S., Bhat, R.B., Tiley, J.S., & Miracle, D.B. (2005). Grain refinement of cast titanium alloys via trace boron addition. Scripta Materialia. 53, 1421-1426.

34. Tamirisakandala, S., Miracle, D.B., Srinivasan, R., & Gunasekera, J.S. (2006). Titanium alloyed with boron. Advanced Materials and Processes. 164 (12), 41-43.

35. Titanium. In Wikipedia. Retrieved June 21, 2015, from https://en.wikipedia.org/wiki/Titanium

36. Tolochko, N.K., Khlopkov, Y.C., Mozzharov, S.E., Lgnatiev, M.B., Laoui, T., & Titov, V. (2000). Absorptance of powder materials suitable for laser sintering. Rapid Prototyping Journal. 6 (3), 155-161.

37. Wang, L., & Thompson, L.T. (1999). Self-propagating high-temperature synthesis and dynamic compaction of titanium boride and titanium carbide. Army Research Laboratory. ARL-CR-440.

38. Wang, X.C., Laoui, T., Bonse, J., Kruth, J.P., Lauwers, B., & Froyen, L. (2002). Direct selective laser sintering of hard metal powders: experimental study and simulation. The International Journal of Advanced Manufacturing Technology. 19, 351-357.

39. Westrum, E.F., & Clay, G.A. (1978). Hypostoichiometric titanium diboride ($TiB_{1.964}$) and hyperstoichiometric tantalum diboride ($TaB_{2.11}$): the heat capacity and thermodynamic properties from 5 to 350 K.

40. Yolton, C.F. (2004). The pre-alloyed powder metallurgy of titanium with boron and carbon additions. JOM. 56, 56-59.

41. Yoshida, W., Kobashi, M., & Kanetake, N. (2007). Synthesis of fine ceramic particles in molten aluminum by combustion reaction. Materials Transactions, 48 (9), 2374-2377.

42. Zeng, K., Pal, D., & Stucker, B. (2012). A review of thermal analysis methods in laser sintering and selective laser melting. Proceedings of Solid Freeform Fabrication Symposium Austin, TX.

43. Zhang, Y., & Faghri, A. (1998). Melting and resolidification of a subcooled mixed powder bed with moving Gaussian heat source. ASME Journal of Heat Transfer. 120, 883-891.

44. Zhang, Y., & Faghri, A. (1999). Melting of a subcooled mixed powder bed with constant heat flux heating. International Journal of Heat and Mass Transfer. 42, 775-788.

BIOGRAPHICAL SKETCH

Yingbin Hu was born on April 21th, 1989 in Shijiazhuang, Hebei, China. His permanent mailing address is: Jinyuan Rd, Zhengding, Shijiazhuang, Hebei, China. And his email address is huyingbin068@gmail.com. Yingbin earned his Bachelor's Degree in Mechanical Engineering in June 2013 from the Shandong University and was selected a member of the Excellent Engineer Class. Yingbin moved to the United States in August 2013 and earned his MS in Manufacturing Engineering from the University of Texas-Pan American in July 2015.

While pursuing his Bachelor's Degree, Yingbin Hu got his chance to attend the National College Students Mathematical Competition (Shandong Division) and won the first prize. When he enrolled as a graduate student, he had the opportunity to work as a graduate assistance for the Manufacturing Department. At the same time, he got the chance to work with selective laser melting machine for research. During the last semester of his master, he received the Academic Deans' Outstanding Student Award.